Properties of Channels Reconstituted from the Major Intrinsic Protein of Lens Fiber Membranes

GEORGE R. EHRING, GUIDO ZAMPIGHI, JOSEPH HORWITZ, DEAN BOK, and JAMES E. HALL

From the Department of Physiology and Biophysics, University of California at Irvine, Irvine, California 92717; and the Department of Anatomy and Cell Biology, Jerry Lewis Center, and the Department of Ophthalmology, Jules Stein Eye Institute, University of California at Los Angeles, Los Angeles, California

ABSTRACT Detergent-solubilized plasma membrane protein of either adult bovine or calf lens and high-performance liquid chromatography-purified major intrinsic protein (MIP) of the lens were reconstituted into unilamellar vesicles and planar lipid bilayers. Freeze-fracture studies showed that the density of intramembrane particles in the vesicles was proportional to the protein/lipid ratio. At high ratios, these particles crystallized into tetragonal arrays as does MIP in lens fibers. Channels induced by either purified MIP or detergent-solubilized protein had essentially identical properties. The conductance of multichannel membranes was maximal near 0 mV and decreased to 0.49 ± 0.08 of the maximum value at voltages >80 mV. The dependence of the conductance on voltage was well fit by a two-state Boltzmann distribution. Voltage steps >30 mV elicited an ohmic current step followed by a slow (seconds) biexponential decrease. The amplitudes and time constants depended on the magnitude but not the sign of the voltage. Steps from 100 mV to voltages <30 mV caused the channels to open exponentially with a millisecond time constant. Analysis of latency to first closure after a voltage step gave nearly the same time constants as multichannel kinetics. Single-channel conductance is proportional to salt concentration from 0.1 to 1.0 M in KCl. In 0.1M KCl, the channel had two preferred conductance states with amplitudes of 380 and 160 pS, as well as three additional substates. Multi- and single-channel data suggest that the channel has two kinetically important open states. The channel is slightly anion selective. The properties of the channel do not vary appreciably from pH 7.4 to 5.8 or from pCa 7 to 2. We propose that a channel with these properties could contribute to maintenance of lens transparency and fluid balance.

INTRODUCTION

The cells of the lens form a functional syncytium. The syncytial properties of the lens have been attributed to the presence of communicating "gap" junctions, located in

Address reprint requests to Dr. George R. Ehring, Department of Physiology and Biophysics, University of California at Irvine, Irvine, CA 92717.

J. GEN. PHYSIOL. © The Rockefeller University Press · 0022-1295/90/09/0631/34 $2.00
Volume 96 September 1990 631–664

the plasma membranes of cells. Gap junctions are composed of discrete channels that directly connect the cytoplasms of adjacent cells. Each channel is constructed of two apposing hemichannels, one per cell, that interact through their external domains to bridge the intervening extracellular space. Therefore, an essential characteristic of cell–cell communication via gap junctions is the exclusion of the extracellular space from the communicating pathway.

Extensive coupling between lens fibers has been demonstrated electrophysiologically and by dye passage (Mathias et al., 1979; Rae, 1979; Scheutze and Goodenough, 1982; Rae and Kuszak, 1983; Miller and Goodenough, 1986). Morphological studies have established that lens fibers contain extensive networks of closely apposed plasma membranes that display the pentalamellar structure associated with gap junctions in transverse sections (Dickson and Crock, 1972; Kuwabara, 1975; Philipson et al., 1975; Benedetti et al., 1976; Zampighi et al., 1982). However, structural studies of lens membranes have demonstrated more junctional heterogeneity than that found in other tissues (Zampighi et al., 1982). In the lens cortex, junctions have greater overall thickness, a flatter surface topology, and a different protein composition than junctions located in the lens nucleus (Simon et al., 1982; Zampighi et al., 1982; Kistler et al., 1985; Gruijters et al., 1987; Zampighi et al., 1989).

The striking structural heterogeneity of lens junctions greatly complicates the identification of the specific structures and proteins responsible for cell–cell communication in the lens. Putative lens junctional proteins include the major intrinsic protein (MIP) of the lens, which predominates in the lens nucleus, and another major protein of M_r 70 kD (MP 70), which is found primarily in the lens cortex. These proteins do not appear to be homologous, but MP 70 has at least partial homology to the liver gap junction protein, and thus may be important in forming gap junctions in the lens (Kistler et al., 1988). Functional studies show that cortical junctions uncouple upon cytoplasmic acidification more readily than nuclear junctions (Scheutze and Goodenough, 1982), indicating that the morphological and biochemical diversity of lens junctions may be reflected in their roles in lens physiology.

Since most of the protein in lens junctions is MIP, it has been proposed as the protein responsible for the syncytial properties of the lens. In favor of this hypothesis is the demonstration that MIP is present in some of the junctional membranes of the lens cortex and most, if not all, of the junctional membranes in the lens nucleus (Bok et al., 1982; Fitzgerald et al., 1985; Sas et al., 1985; Zampighi et al., 1989). Also, the amino acid sequence of MIP deduced from its cDNA clone is consistent with that of a membrane-spanning protein (Gorin et al., 1984). Protein solubilized from lens plasma membranes enriched for MIP and reconstituted into planar lipid bilayers (BLM) forms voltage-dependent channels (Zampighi et al., 1985; Ehring and Hall, 1988, 1989; Ehring et al., 1988). These channels are qualitatively similar to those described in reconstitution experiments with rat liver gap junction proteins (Spray et al., 1986; Young et al., 1987). In addition, solubilized lens proteins alter the permeability of unilamellar liposomes to molecules <1 kD in molecular mass (Girsch and Peracchia, 1985*a*, *b*; Nikaido and Rosenberg, 1985; Gooden et al., 1985*a*, *b*; Peracchia and Girsch, 1985; Scaglione and Rintoul, 1989).

However, other experimental data reveal substantial differences between junctions containing MIP and gap junctions composed of other proteins. First, immunocytochemical studies have shown that MIP is localized to single plasma membranes in addition to its presence in junctional membranes (Fitzgerald et al., 1983, 1985; Paul and Goodenough, 1983). In contrast, gap junctional proteins in other tissues (the connexin superfamily) have not been shown to be in single membranes. Secondly, the amino acid sequence of MIP shows no homology to the sequences of gap junction proteins from other tissues (Hertzberg et al., 1982; Nicholson et al., 1983; Gorin et al., 1984; Kumar and Gilula, 1986; Paul, 1986; Kistler et al., 1988). Thirdly, junctions located in the lens nucleus, which contain principally MIP, are 11–13 nm thick, whereas gap junctions are 15–17 nm thick (Zampighi et al., 1980, 1982, 1989). Fourthly, RNA transcribed from the cDNA of MIP does not increase coupling between pairs of injected *Xenopus* oocytes whereas injection of RNA transcribed from the cDNA of rat liver gap junction protein does increase the coupling between oocyte pairs (Dahl et al., 1987; Ebihara et al., 1989; Swenson et al., 1989). Fifthly, immunocytochemistry and label-fracture techniques demonstrate that MIP does not form coaxially aligned gap junction channels (Zampighi et al., 1989). These functional and structural differences suggest that if MIP contributes to cell–cell communication, it does so by a mechanism different from gap junctions.

In this article, we present evidence that MIP forms the channels seen upon incorporation into bilayers; we present a detailed characterization of the voltage-dependent properties of the channels; and we use these properties to propose a new model to explain the role of MIP in creating the syncytial properties of the lens. This model predicts that cell–cell communication mediated by MIP involves the extracellular space. The model also suggests that MIP has a role in minimizing extracellular space and maintaining transparency in the lens.

MATERIALS AND METHODS

Isolation Methods

Membrane isolation. Lenses from 3-mo-old calves or adult cows, quick frozen under liquid nitrogen at the slaughterhouse and shipped on dry ice, were obtained from Pel-Freeze Biologicals (Rogers, AR). Lens plasma membranes were isolated with slight modifications of the methods of Zampighi et al. (1982). After removal of their capsules, approximately 50 lenses were cut into small pieces with a razor blade and homogenized in about 300 ml of solution A (2 mM $NaHCO_3$, 3 mM EDTA, 100 μM phenylmethylsulfonyl fluoride, 0.08 μM aprotinin, 1.0 μM pepstatin, 1.0 μM leupeptin; the final pH of solution A was adjusted to 8.0 with NaOH). The homogenate was diluted to 1 liter with solution A, filtered through surgical gauze, and then centrifuged at 2,000 *g* for 10 min. The pellets were washed and concentrated in two steps (to 750 ml and then 500 ml of solution A) by resuspension and centrifugation. After the second wash in solution A, the pellets were transferred to 500 ml of solution B (4 mM Tris base, 5 mM EDTA, 1 mM $CaCl_2$, and 1.5 mM NaN_3, 100 μM phenylmethylsulfonyl fluoride, 0.08 μM aprotinin, 1.0 μM pepstatin, 1.0 μM leupeptin; the final pH of solution B was adjusted to 8.0 with NaOH) and centrifuged at 2,000 *g* for 10 min. The pellets were extracted with 500 ml of 4 M urea in solution B and centrifuged at 17,000 *g* for 20 min. The pellets were extracted a second time using 150 ml of 7 M urea in solution B and centrifuged at 64,000 *g* for 90 min. The pellets were resuspended and washed three times in solution B by

centrifugation at 17,000 *g* for 10 min. After each centrifugation, the dark central portion of the pellet was discarded. The isolated membrane preparation was diluted to 1–3 mg/ml in solution C (200 mM NaCl, 4 mM Tris base, 5 mM EDTA, 1 mM $CaCl_2$, and 1.5 mM NaN_3, made up with 20% glycerol and final pH adjusted to 8.0 with NaOH) and stored at −70°C. Protein concentration was determined by a modified Lowry assay (Lowry et al., 1951) (Sigma Chemical Co., St. Louis, MO).

High-performance liquid chromatography purification. MIP was purified from isolated membranes using high-performance liquid chromatography (HPLC). Approximately 4 ml of the isolated lens membrane preparation (protein concentration 3 mg/ml) was centrifuged at 15,000 *g* for 15 min. The pellet was solubilized overnight at 4°C in 4 ml of 50 mM sodium phosphate buffer, pH 7.9, containing 2% octyl-β-D-glycopyranoside (OG) and 1 mM sodium azide. This solution was centrifuged at 200,000 *g* for 20 min; 500-μl aliquots of the supernatant were applied to a chromatograph (model 100A, Beckman Instruments, Inc., Palo Alto, CA) equipped with a silica gel filtration column (Toyosoda model 3000, TSK America Inc., North Bend, WA). The column was equilibrated with sodium phosphate buffer containing 1% octyl β-D-glucopyranoside. The flow rate for the HPLC was 0.5 ml/min and 1.0-ml fractions were collected. The fractions that eluted from the column with retention times of 13, 22, 26, and 33 min showed strong absorbance at 280 nm as determined with an absorbance detector (model 160, Beckman Instruments Inc.). After eight runs, the total volume collected for each of the fractions was combined and concentrated by centrifugation at 5,000 *g* using microconcentrator tubes (Centricon-10, Amicon Corp., Danvers, MA). As described in the results, the fraction that eluted with a retention time of 26 min contained the most highly purified MIP. From the eight runs, a total of 375 μg MIP was contained in this fraction, resulting in a 3% yield.

The protein compositions of the urea-washed calf lens membranes and the HPLC fractions were determined on a 12% SDS polyacrylamide gels following the methods of Laemmli (Laemmli, 1970), except that MIP was solubilized at 40°C (Wong et al., 1978). Protein bands on the polyacrylamide gel were visualized by silver stain (Polysciences, Inc., Warrington, PA).

Immunoblots. We tested for the presence of MIP and MP70 in the lens membrane isolate and HPLC fractions; the proteins from the slab gel were transferred to nitrocellulose following the methods of Burnette (Burnette, 1981). The nitrocellulose replicas were mounted in a plexiglass chamber (Miniblotter 45, Immunetics, Cambridge, MA), for simultaneous probing with monoclonal antibodies directed against MIP (a gift from Drs. D. Paul and D.A. Goodenough, Department of Anatomy and Cell Biology, Harvard Medical School) and MP 70 (a gift from Dr. J. Kistler, Department of Cell Biology, Univesity of Auckland). The blots were stained with anti–mouse IgM linked to horseradish peroxidase (Sigma Chemical Co.). The peroxidase reaction was carried out with hydrogen peroxide as the substrate and 4-chloro-1-naphthol as the chromophore.

Reconstitution Methods

Vesicle formation and freeze-fracture. MIP was reconstituted into small unilamellar vesicles using previously published methods (Zampighi et al., 1985). For the electrophysiological experiments, the mole ratio of MIP to phosphatidylcholine in the vesicles was varied from 1:1000 to 1:10,000. To obtain these ratios, aliquots containing 7–70 μg of HPLC-purified MIP or aliquots containing 10–100 μg of total protein from our lens junctional membrane preparation solubilized in solution C containing 470 mM octyl β-D-glucopyranoside were combined with 2.5 μmol of phosphatidylcholine (Avanti Polar Lipids, Inc., Birmingham, AL) also solubilized in solution C with 470 mM octyl β-D-glucopyranoside. A total volume of 0.5 ml of the phosphatidylcholine protein-octyl β-D-glycopyranoside solution was placed in a dialysis bag with an M_r cutoff of 3.5 kD (Spectrum Medical, Los Angeles, CA) and then dialyzed twice

against 3 liters of a solution containing 200 mM NaCl and 25 mM *N*-tris(hydroxymethyl)-methyl-2-animoethane sulfonic acid, titrated to a final pH of 7.0 with NaOH. MIP reconstituted in vesicles as described above but at protein/lipid ratios of 1:20,000; 1:400, or 1:100 (mol/mol) was studied by conventional freeze-fracture electron microscopy as described previously (Zampighi et al., 1985).

Bilayer Methods

Bilayer formation. Bilayers were formed in Teflon chambers divided into two compartments each having a volume of 2 ml. The compartments were separated by a 20-μm-thick Teflon partition with a 200-μm hole (pretreated with approximately 0.5 μl of squalane (Atomergic Chemicals Corp., Plainview, NY)) (Montal and Mueller, 1972; Hall et al., 1984). With the aqueous solutions below the hole, 10 μl of 5 mg/ml phosphatidylethanolamine (Avanti Polar Lipids, Inc.), dried under argon and dissolved in pentane (HPLC, Aldrich Chemical Co., Milwaukee, WI) were spread over the aqueous phase. To form the bilayers, the solutions in the compartments were slowly raised over the hole.

Bilayers generally formed within 5–10 min after raising the phosphatidylethanolamine monolayers over the hole. Bilayer formation was detected as an increase in capacitance across the partition. The bilayers in these experiments had a mean capacitance of 360 ± 130 pF (~0.5 $\mu F/cm^2$) and a conductance of less than 10^{-11} S (specific resistance approximately 10^8 Ω-cm^2).

Channel incorporation. The kinetics and the voltage dependence of reconstituted MIP channels were studied principally in two solutions: (*a*) 1 M KCl with 20 mM 2-(*N*-morpholino)ethanesulfonic acid (MES) buffered to pH 5.8 with KOH, and (*b*) 1 M KCl with 10 mM *N*-2-hydroxyethylpiperazine-*N*′-2-ethanesulfonic acid (HEPES) buffered to pH 7.4 with KOH. The ionic strength and selectivity experiments were performed with 0.2 or 0.1 M KCl with 20 mM MES, ph 5.8. Additional experiments were performed with 1.0 or 0.1 M NaCl with 10 mM HEPES buffered to pH 7.4 with NaOH.

In most cases channels were observed in the BLM after bilateral addition of aliquots (1–10 μl) of the small unilamellar vesicles containing octyl β-D-glucopyranoside solubilized lens membrane protein or HPLC-purified MIP to the solution bathing the membrane. The average time to the appearance of the first channel was 40 ± 18 min after bilateral addition of vesicles with a MIP phosphatidylcholine ratio of 1:10,000 and 27 ± 12 min with a MIP phosphatidylcholine ratio of 1:1,000. In five experiments where vesicles were added to only one of the compartments of the bilayer chamber; no incorporation was observed for 1 h after unilateral addition. However, in one of these experiments a single channel was seen in the membrane 2 h after the unilateral addition of vesicles.

Voltage clamp. The voltage clamp apparatus used in this study has been previously described (Hall et al., 1984). Briefly, one compatment of the bilayer chamber was clamped to virtual ground with a high-input impedance current to voltage transducer. The *I-V* transducer had an adjustable feedback resistor (10^6 to 10^8 Ω). A command potential (V_c) was applied to the opposite bilayer compartment by either a microcomputer driven digital-to-analog converter or a battery-driven potentiometer. The current that flowed across the membrane was collected and digitized with a 12 bit analog-to-digital converter. Current–voltage curves were recorded on an X-Y plotter (model 7034A, Hewlett-Packard Co., Palo Alto, CA) and single-channel currents at constant applied voltage were stored on magnetic tape at a bandwidth of 5 kHz.

Two basic voltage clamp protocols were used. (*a*) Step protocol: the membrane was held at holding potential (V_h), usually 0 mV, and then stepped to a command potential (V_c) and the current response at V_c was measured. (*b*) Ramp protocol: starting from a holding potential of 0 mV the membrane voltage was first swept in the positive direction to 100 mV then the

direction of the voltage ramp was reversed and the membrane voltage was swept in the negative direction to −100 mV and finally back to the holding potential at a constant rate of 10 mV/s.

Data analysis and computer programs. Data are presented as the mean ± the standard error of the mean. Statistical comparisons of group means were performed using Student's *t* test. Single and double exponential fits were done with nonlinear least squares fitting routine (Clampfit, Axon Instruments, Foster City, CA). Single-channel analysis was accomplished by playing the recorded data to an analog-to-digital converter under the control of commercially available software (PCLAMP, Axon Instruments, Inc., Foster City, CA). Single-channel data was filtered a 1 kHz with a eight-pole Bessel filter (Frequency Devices, Haverhill, MA). Fits of the Boltzmann distribution to the conductance-voltage data were accomplished with a nonlinear fit using a Marquardt-Levenberg algorithm programmed in Fortran (Bevington, 1969).

RESULTS

Characterization of the Lens Membrane Preparation and HPLC-purified MIP

Protein composition. Plasma membrane proteins isolated from calf lenses exhibited approximately 14 bands on SDS-PAGE gels. Apparent M_r ranged from 14 to 96 kD (Fig. 1, lane *A*). Two lens membrane proteins, MIP (26 kD) and MP 70 (70 kD) are of special interest because they are components of lens junctions and could play a role in lens cell communication. Immunoblots with anti–MIP and anti–MP 70 monoclonal antibodies confirmed the presence of MIP (Fig 1, lane *C*) and MP 70 (Fig 1, lane *E*) in the calf lens membrane isolate. MIP was further purified using HPLC silica gel-filtration techniques. Of the four eluted fractions with significant absorbance at 280 nm, the fraction with a retention time of 26 min showed the greatest enrichment for MIP in silver-stained SDS gels loaded with 1 μg of protein (Fig. 1, lane *B*). Optical density scans of the gel demonstrated that MIP constituted >99% of the protein in this fraction. Possible contaminant bands were observed only at the limit of resolution of the silver staining technique, which is on the order of nanogram amounts of protein. MP 70 was not detectable in the silver stain of the 26-min fraction. Immunoblots confirmed the presence of MIP (Fig. 1, lane *D*) in this fraction while the amount of MP70 was undetectable with this technique (Fig. 1, lane *F*).

Freeze-fracture analysis of vesicles containing MIP. Vesicles formed in the presence of MIP contained distinct intramembrane particles 6–7 nm in diameter that cast shadows on otherwise smooth fracture faces. The particle density increased with the protein/lipid ratio of the vesicles. Vesicles prepared with a ratio of 1:20,000 (mol/mol) contained on average two particles per vesicle (Fig. 2 *A*). Vesicles prepared with a ratio of 1:400 (mol/mol) contained numerous particles, some of which formed plaques (arrows in Fig. 2 *B*). At a lipid/protein ratio of 1:100 (mol/mol), the particle density was sufficient to promote crystallization (Fig. 3 C). Initially, a very high uniform density of particles and pits was observed in the fracture face (Fig. 3 *A*). With time, the particles aggregated leaving extensive regions of the vesicle displaying a smooth fracture face (Fig. 3 *B*). Small crystalline arrays appeared inside these aggregates (circles in Fig. 3 *B*). As these arrays grew larger,

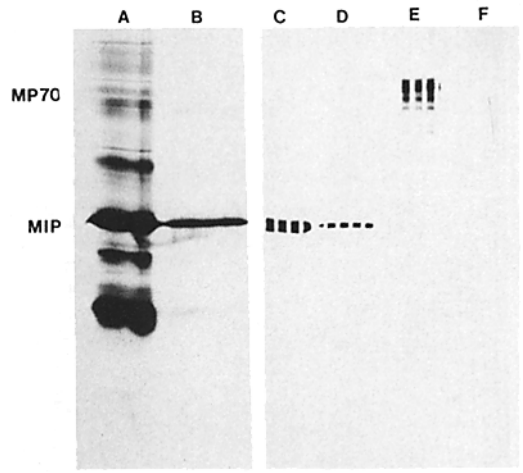

FIGURE 1. Comparison of SDS-PAGE and immunoblots on the total protein from isolated calf lens membranes (lanes *A,C,E*) and HPLC-purified MIP (lanes *B,D,F*). A 12% polyacrylamide gel was loaded with ~1 μg of protein and silver stained. Calf lens membrane isolate contained at least 14 protein bands (lane *A*) with M_r in the range of 14–96 kD. In contrast, a fraction that eluted from the HPLC after a retention time of 26 min contained one predominant band with an M_r of 26 kD (lane *B*). Note: Several faint bands, which did not reproduce photographically, were discernible on the gel. These bands indicated contaminants present in amounts on the order of the nanogram resolution of the silver staining technique. Lanes *C–F* are immunoblots against anti-MIP (lanes *C* and *D*) or anti–MP 70 monoclonal antibodies (lanes *E* and *F*). The antibodies were visualized with anti–mouse, anti–IgM antibody linked to horseradish peroxidase. Positive reactions are indicated by small rectangular spots on the nitrocellulose paper, four to five spots per lane. Immunoblots of the protein isolated from calf lens membrane demonstrated the presence of both MIP (lane *C*) and MP 70 (lane *E*). The HPLC fraction was labeled with anti–MIP antibody (lane *D*); however, MP 70 was undetectable with the immunoblot (lane *F*).

they began to display a tetragonal symmetry with 6.6-nm unit cell dimension (Fig. 3 *C*).

Freeze-fracture experiments performed on vesicles reconstituted at different lipid/protein ratios provided three characteristics of reconstituted MIP: (*a*) the density of particles was proportional to the amount of protein used during the reconstitution (Figs. 2 and 3). This implies that MIP forms the particles and therefore is a transmembrane protein. (*b*) Particles and pits coexisted in the same fracture face suggesting that the insertion of MIP occurs with random orientation. (*c*) MIP crystallized into tetragonal arrays with symmetry and unit cell dimensions identical to those observed in lens fibers (Simon et al., 1982; Zampighi et al., 1982). These observations imply that each channel is a tetramer of MIP.[1]

[1]The tetrameric form of MIP channels can be established by the following calculations: From the measured ratios of protein, phospholipid and cholestrol in isolated membranes one can estimate a molar ratio of 20 phospholipids and 15 cholesterol molecules per MIP (Zampighi et al., 1982). The volume of each MIP monomer is 36.5 nm^3 (0.0013 nm^3 per dalton). The average volume of a lipid molecule is 1 nm^3 estimated by multiplying the partial molar area (0.43 nm^2) by one half the thickness of a bilayer having the given composition (2.4 nm). Thus, a volume of about 71 nm^3 is obtained for each MIP and its complement of 35 lipids. The volume of the unit cell (269–292 nm^3) is calculated by multiplying the area of the unit cell (6.7 $nm)^2$ by one half the thickness of the junction (6–6.5 nm). The number of MIP molecules per unit cell is estimated by dividing the volume of the unit cell by the volume of one MIP monomer plus its 35 lipid complement (269–292/71 = 3.8–4.1). Therefore, MIP in the tetragonal arrays of isolated membranes is a tetramer. tetramer.

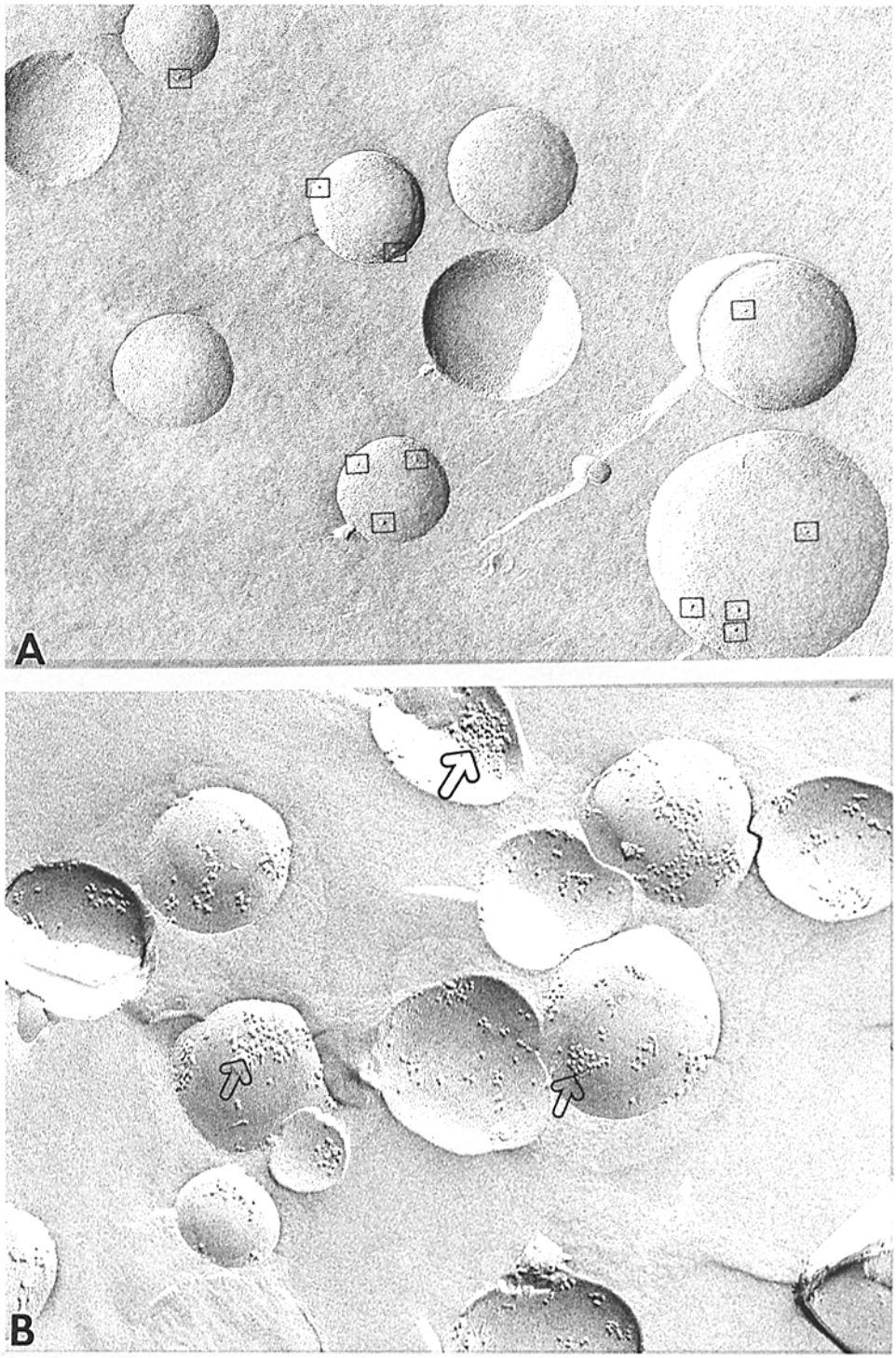

FIGURE 2.

Comparison of channels reconstituted from isolated lens membranes and HPLC-purified MIP. The voltage dependence of the reconstituted channels was assayed by monitoring the current flowing across the bilayer in response to triangular voltage ramps. Fig. 4 demonstrates that channels induced in BLMs by vesicles containing either total solubilized lens membrane protein or the HPLC-purified MIP had identical single-channel conductance and voltage dependence.

Fig. 4, *A* (OG-solubilized lens membrane) and *C* (HPLC-purified MIP), shows continuous *I-V* curves taken after the incorporation of a single channel into the BLM. The current observed in both cases was linearly proportional to voltage in the range of −30 to +30 mV with a conductance of 3.7 nS (in 1 M KCl, pH 5.8). As the absolute value of the voltage was increased beyond this range the noise on the current trace increased until discrete current steps reflecting channel closures were observed at +37 and −40 mV in Fig. 4 *A* and +70 and −60 mV in Fig. 4 *C*. When the channel "closed," the conductance of the bilayer did not decrease to the bare bilayer value (10 pS), but rather to ~1.6 nS. Thus, the channel had at least two open states.

I-V curves from many-channel membranes (Fig. 4, *B* and *D*) displayed voltage dependence similar to that of single-channel membranes. In multichannel membranes two major conductance states were apparent, G_{max}, the maximum observed conductance and, G_{min}, the minimum observed conductance. G_{max} was measured as the conductance at voltages between −30 mV and +30 mV and G_{min} as that near 100 mV.

In control experiments (data not shown), vesicles made without MIP, or with MIP denatured by heating or treatment with SDS did not induce the incorporation of voltage-dependent channels in BLM. Addition of vesicles containing MIP partially digested with trypsin resulted in the incorporation of channels with a reduced voltage dependence.

Voltage Dependence of the MIP Channel

Multichannel conductance measurements. We examined the relationship of G_{min} to G_{max} to determine if the conductance was the result of one type of channel with two primary open conductance states or several types of channels, one voltage-dependent and one more voltage-independent, which rarely if ever closed. If there is only one type of channel with two conductance states, then G_{max} in a multichannel membrane would be a constant multiple of G_{min}. Thus, the ratio of G_{max} to G_{min} would be independent of the number of channels in the BLM. If, however, the

FIGURE 2. (*opposite*) Dependence of the density of transmembrane particles on protein/lipid ratio. (*A*) Freeze-fracture replica of vesicles formed at a low ratio (1:20,000 mol/mol). The presence of MIP in the reconstitution resulted in the appearance of 6–8-nm diameter particles, which cast shadows on the otherwise smooth fracture faces of the vesicles (□). The conditions used in this reconstitution produced an average of two particles per vesicle. (*B*) Vesicles formed at a higher protein/lipid ratio (1:400 mol/mol). The increase in MIP concentration resulted in a higher particle density. In some vesicles, the particles formed clusters (*arrow*), a fact that did not permit the quantification of the particle density. ×100,000.

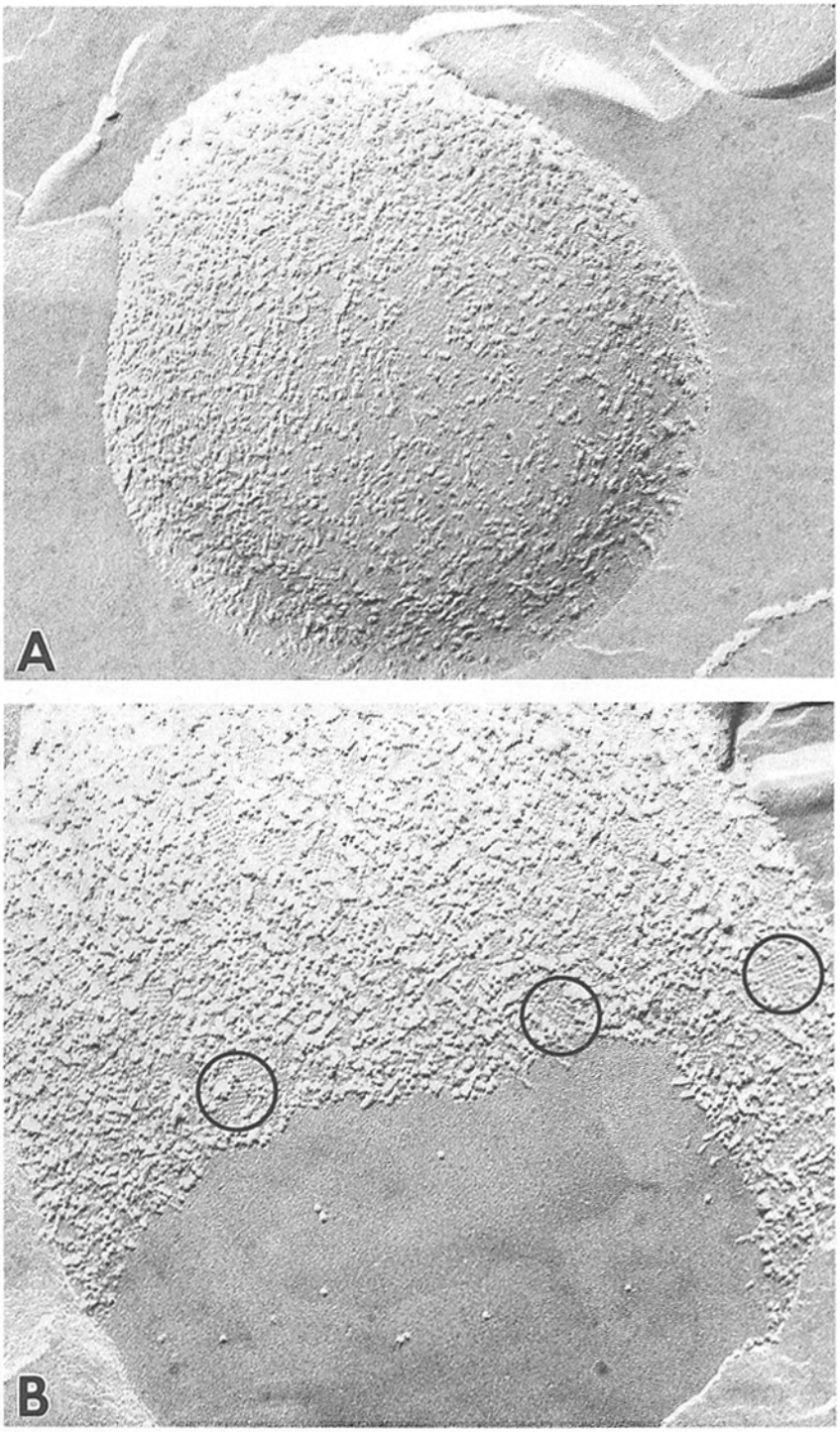

FIGURE 3.

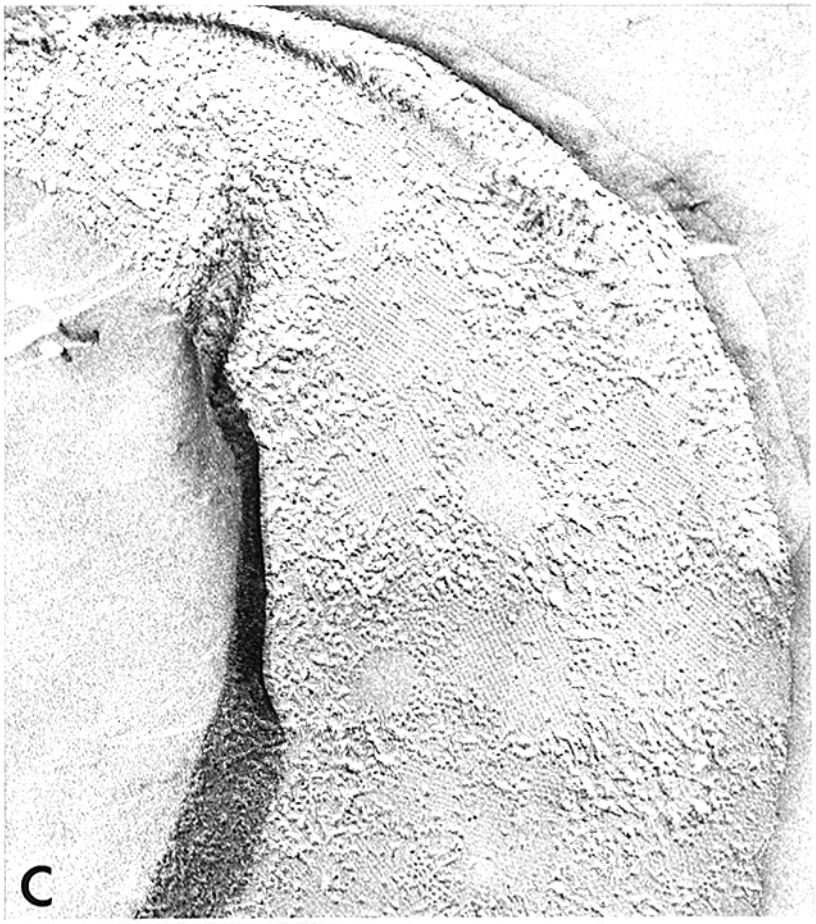

FIGURE 3. Development of crystalline arrays of MIP with high protein/lipid ratios. The density of intramembrane particles increased markedly when the protein to lipid ratio was increased to 1:100 (mol/mol). (*A*) Vesicle of approximately 0.8 μm in diameter, which was twice the diameter of vesicles formed at lower protein to lipid ratios. These vesicles contained a high concentration of particles distributed in the convex fracture face. Incubation of the vesicles produced self-aggregation of the particles. (*B*) Large vesicle displaying particles aggregated into clusters and separated by regions containing pits. These pits are arranged in straight lines indicating the formation of crystalline arrays. Also shown in this vesicle is an extensive smooth fracture face containing only a few scattered particles. The area devoid of particles probably results from the fact that particle clusters occupy less surface area. An important characteristic of these vesicles is the coexistence of particles and pits in the same fracture face; an observation suggesting random insertion of protein into the lipid bilayer. (*C*) Vesicle of the same preparation in which MIP crystallized into larger arrays. These arrays display tetragonal symmetry with a 6.6-nm unit cell dimension. Thus, they are identical to the arrays of MIP demonstrated in freeze-fracture studies of isolated lens fiber membranes and whole lens. Therefore, under the conditions used for our reconstitutions at least a fraction of the MIP molecules return to the tetrameric form seen in native membranes. ×100,000.

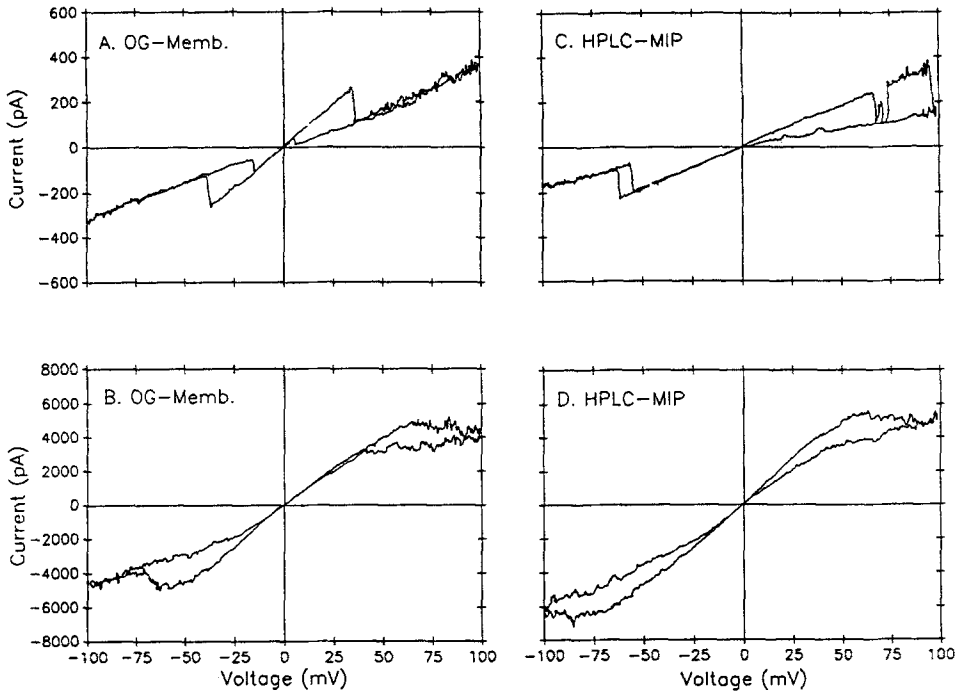

FIGURE 4. *I-V* curves of channels reconstituted from solubilized lens membrane protein (*left panels*) and by HPLC-purified MIP (*right panels*) in response to triangular voltage ramps. At a constant rate of 10 mV/s, the membrane voltage (V_c) was first increased to +100 mV from a holding potential of 0 mV; at 100 mV, the direction of the voltage ramp was reversed and V_c was swept to −100 mV; at −100 mV, the direction of the ramp was reversed and membrane voltage was returned to the holding potential. During the application of the voltage ramp, membrane voltage and current were continuously plotted on an X-Y recorder. Channels reconstiuted into BLMs using vesicles containing either octyl β-D-glucopyranoside solubilized protein from calf lens membrane (OG-Memb) or HPLC purified MIP (HPLC-MIP) had identical voltage dependences and single-channel conductances. In membranes containing only a single-channel (*A* and *C*), the channels were open near 0 mV with a conductance of 3.6 nS in 1 M KCl/20 mM MES buffered to pH 5.8. Discrete channel closings were seen as the voltage was swept positive or negative from zero (for example at +37 and −40 mV in *A* or at +70 and −60 mV in *C*). The channels closed to a minimum conductance state, which was ~1.6 nS. In multichannel membranes (*B* and *D*) the membrane current was linearly proportional to voltage in the range of −30 to +30 mV, but at larger membrane voltages this relationship deviated from linearity, reflecting a voltage-dependent decrease in membrane conductance.

current passes through different types of channels, then the ratio of G_{max} to G_{min} would depend on the proportions of channel types present.

In 169 reconstitutions, performed in 1 M KCl and using a variety of lens fiber membrane preparations, the ratio of G_{max} to G_{min} was constant over four orders of magnitude in conductance (Fig. 5). The relationship of G_{max} to G_{min} was fit by the

linear regression:

$$G_{max} = 1.91 \pm 0.01 * G_{min} + 1.65 \pm 12.86 \qquad R^2 = 0.999.$$

The strong correlation of G_{max} to G_{min} over this large number of reconstitutions in which the final conductance of the membrane varied over such a wide range suggests that both G_{max} and G_{min} are fundamental properties of the same MIP channel. These experiments do not rule out the possibility that a voltage-dependent channel and one or more voltage-independent channels are isolated together, co-purify, run identically on HPLC gel filtration columns and SDS gels, and incorporate into BLMs with a constant stoichiometry. This, however, seems unlikely.

Steady-state conductance vs. voltage. The voltage-dependent closure of MIP channels was studied in membranes containing many channels by examining mem-

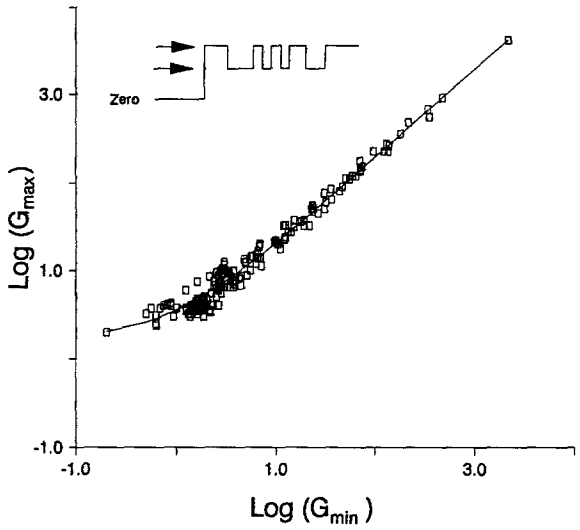

FIGURE 5. Maximum (G_{max}) and minimum (G_{min}) conductances for membranes with reconstituted MIP channels were determined from *I-V* curves. In 169 reconstitutions, G_{max} was a constant multiple of G_{min} (□) and the relationship between G_{max} and G_{min} could be fit by the linear regression (*solid line*): $G_{max} = 1.91 \pm 0.01 * G_{min} + 1.65 \pm 12.86$, $R^2 = 0.999$. (*Inset*) Single-channel current transitions for a model of the MIP channel, which has two primary open conductance states (*arrows*). The channel transitions from the high to the low conductance state in response to increased membrane voltages, but does not close to the bare bilayer conductance level (essentially zero at the conductance scale shown).

brane-current responses to voltage pulses. When the membrane-voltage was stepped from a holding potential (V_h) of 0 mV to a test potential (V_c) in the range of ±100 mV, the initial current response (I_0) was a linear function of voltage and was proportional to G_{max}, the conductance of the membrane near 0 mV. If the membrane was held at voltages with absolute values >30 mV, the current declined from I_0 with an exponential time course of many seconds until it approached a nonzero steady-state current (I_{ss}). The steady-state conductance at the end of the test pulse (G_{ss}), defined as I_{ss}/V_c, was a nonlinear function of voltage. Fig. 6 shows the normalized steady-state conductance (G_{ss}/G_{max}) plotted aganist V_c for 12 membranes each of which had at least 15 channels. The conductance was maximal near 0 mV and approached a minimum value of 0.5 at 100 mV. A two-state Boltzmann

distribution was fit to this data using the equation:

$$G_{ss}/G_{max} = \frac{\exp[-n(V - V_0)/kT] + (G_{min}/G_{max})}{\exp[-n(V - V_0)/kT] + 1},$$

where G_{min}/G_{max} is the ratio of the steady-state conductance at large voltages to the conductance near zero mV, n is the apparent gating charge for the channel in units of electron charge (e), and V_0 is the voltage at which the conductance of the channel equals $(G_{max} + G_{min})/2$ (Spray et al., 1981). Parameter values of $G_{min}/G_{max} = 0.49 \pm 0.08$, $n = 2.61 \pm 0.57\ e$ and $V_0 = 57 \pm 9$ mV fit the data from 12 experiments using HPLC-purified MIP. The fit of the data by this two-state model implies that the two open conductance states observed during the continuous current–voltage ramps are the most prevalent conductance states for the channel. In eight experiments with channels reconstituted from the lens plasma membrane preparation the values for G_{min}/G_{max} (0.48 ± .08) and V_0 (65 ± 10 mV) were not significantly different from the

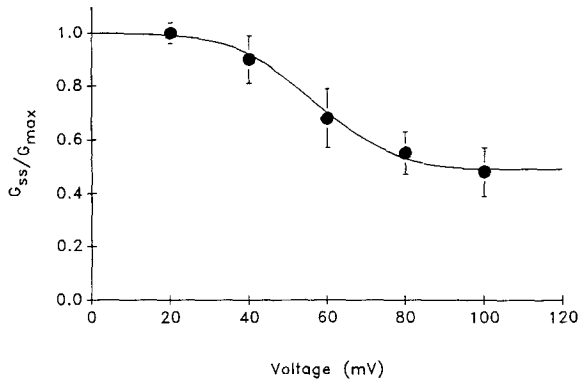

FIGURE 6. Voltage dependence of the conductance of MIP channels. The mean and standard error ($n = 12$) of steady-state conductances, obtained at membrane voltages from 0 to 100 mV, was plotted against voltage (●). The steady-state conductance (G_{ss}) was calculated from the current at the end of an 11.5-s voltage pulse (see inset to Fig. 7) and normalized against the conductance at the beginning of the pulse (G_{max}). The solid lines shows predicted conductance values for a two-state channel. Best fit values of the parameters for the Boltzmann relationship described in the text were: $G_{min}/G_{max} = 0.49 \pm 0.08$, $n = 2.61 \pm 0.57\ e$ and $V_0 = 57 \pm 9$ mV.

values obtained with the HPLC-purified MIP. The voltage dependence of channels reconstituted from the lens membrane preparation was not as steep ($n = 1.9 \pm 0.76\ e$) as that of the channels reconstituted from HPLC-purified MIP ($P < 0.05$). This difference could be the result of the presence of endogenous proteolytic degradation products of MIP in the membrane preparation, but not in the HPLC-purified preparations.

Channel gating: off-kinetics. The time course of the current decrease from I_0 to I_{ss} was well fit by two exponentials; one with a fast (I_f) and one with a slow (I_s) time constant. The currents were symmetric with respect to the sign of V_c (Fig. 7). Pulses to +20 or −20 mV resulted in a step increase in current which remained essentially constant throughout the test pulse. However, during test pulses to larger membrane voltages a decrease from the initial current was evident. The time constants obtained by fitting a double exponential curve to the experimental data were identical for a given amplitude of V_c regardless of the sign of the voltage. The time constants for (I_f)

decreased from 1.8 s at 40 mV to 0.3 s at 100 mV while those for (I_s) changed from 12 to 5 s over the same voltage range (Fig. 8, *b*, and *c*; and Table I).

In addition to the dependence of the two time constants on V_c, the amplitudes of the two components of the voltage-dependent current were also affected by the membrane voltage. The relative contribution of I_f to the total voltage-dependent current increased from about 25% to 50% while that of I_s decreased from 75% to 50% as the membrane voltage increased from 40 to 100 mV (Fig. 8 *a*; Table I). Thus, at higher voltages the time course for the relaxation of the current was shortened by

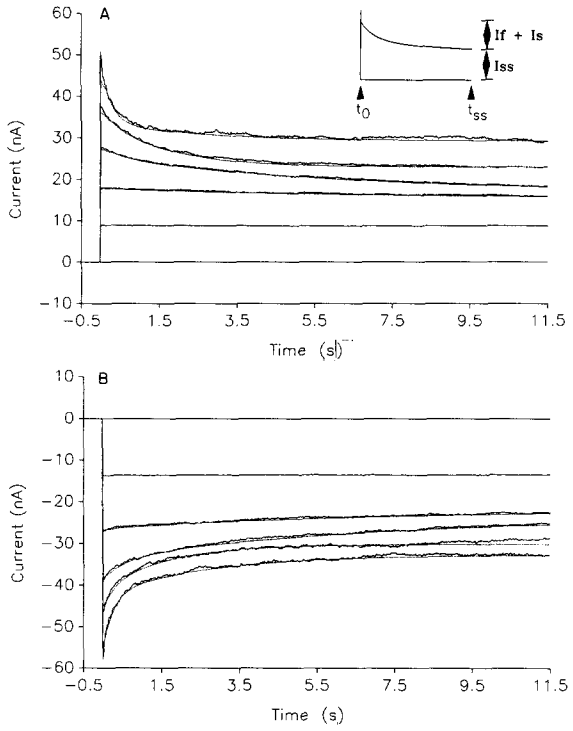

FIGURE 7. Currents through MIP channels were symmetric both in amplitude and time course during pulses to positive voltages (*A*) and negative voltages (*B*). The current measured immediately after the application of the voltage pulse (at t_0) was a linear function of voltage and proportional to G_{max}, the conductance at 0 mV. When V_c had an absolute value >30 mV the current decreased exponentially with time until it reached steady state. Thus, the total current could be fit with a double exponential according to the equation: $I = I_f * \exp(-t/\tau_f) + I_s * \exp(-t/\tau_s) + I_{ss}$. Least-squares fits using this equation are shown overlaying the data traces for pulses to ±40, 60, 80, and 100 mV. The time constants and amplitudes for the fast and slow components of the current as well as the steady-state conductance values were identical for both positive and negative pulses (see also Table I). (*Inset*) Definitions of the terms used in this figure: t_0 and t_{ss} are the times at the onset and end of the pulse respectively; I_f is the fast component, I_s the slow component and I_{ss} the steady-state component of the current.

a decrease in both the time constants and by an increase in the contribution of the fast process to the total current change.

Channel gating: on-kinetics. In contrast to the slow turn-off of the channels at large membrane voltages (time constants on the order of seconds), the channels open rapidly on the return to smaller membrane voltages (time constants on the order of milliseconds). After a 10-s conditioning pulse to 110 mV, during which the conductance of the membrane declined to G_{min}, a 50-ms test pulse to 10 mV resulted in a complete return of the membrane conductance to G_{max}. Fig. 9 shows the time

course of the conductance increase during a test pulse to 10, 30, 50, or 70 mV. The conductance increases measured at these voltages were well fit by single exponentials with voltage-dependent time constants; 0.3 ms at 10 mV, 3.0 ms at 30 mV, 7.8 ms at 50 mV, and 9.3 ms at 70 mV. In three similar experiments, the mean time constants for the recovery process were 10.7 ± 0.4 ms at 50 mV and 3.04 ± 0.3 ms at 30 mV. When test pulses with the opposite sign of voltage from the prepulse were used, the conductance increase was complete by the end of the capacitive transient. Thus, only an upper limit of 0.3 msec can be assigned to the recovery time constant.

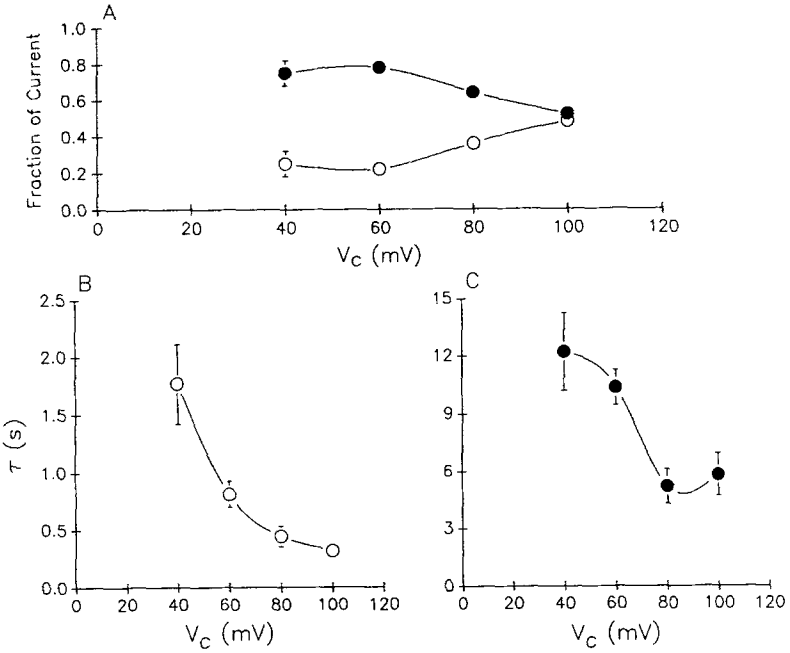

FIGURE 8. Summary of the effects of voltage on the fast and slow components of the MIP currents. (*A*) The fraction of the total current relaxation contributed by the slow component decreased from 75% to 50% (●) and the fraction contributed by the fast component (○) increased from 25% to 50% as V_c increased from 40 to 100 mV. (*B*) Time constant for the fast component decreased from 2 to 0.4 s as V_c increased from 40 to 100 mV. (*C*) Time constant for the slow component also decreased (from 12 to 4 s) over the same voltage range.

Single-Channel Results

Single-channel currents. Single-channel currents in response to voltage pulses demonstrated a behavior similar to that of the multi-channel currents. Pulses to positive or negative potentials resulted in symmetric current responses with respect to "open-channel" (maximum) currents and "closed-channel" (minimum) currents. Fig. 10 demonstrates the symmetry of channel closures after test pulses in the range −80 to +80 mV. The current steps at all voltages were consistent with a channel that had two major conductance states. In addition to the major channel transition,

closures to possible subconductance states occurred during the steps of ±40 or 60 mV. These transitions were also observed on steps to ±80 mV as well as brief transitions towards zero current. However, no stable channel state at the zero current level was observed.

The data in Fig. 10 also show that the time between the step to V_c and the first channel closure decreased as the voltage increased. Moreover, the frequency of channel closings and the duration of those closings increased with the amplitude of the membrane voltage. These three kinetic parameters were symmetric with respect to the sign of V_c. Thus, the kinetic behavior observed in single-channel membranes was consistent with that seen in multi-channel membranes.

Single-channel conductance histograms. Conductance histograms were constructed from the current responses to a series of five test pulses each to 40, 60, or 80 mV. These histograms illustrate that MIP channels have two preferred conductance states and that the probability of occupancy for each state is steeply affected by

TABLE I

Voltage Dependence of the Time Constants and Amplitudes of the Slow and Fast Components of the Current

V_c	$I_f/(I_f + I_s)$	τ_f	$I_s/(I_f + I_s)$	τ_s	I_{ss}/I_0	n
1 M KCl, 20 mM MES, pH 5.8						
mV		*s*		*s*		
20	—	—	—	—	1.00	15
40	0.25 ± 0.07	1.77 ± 0.35	0.75 ± 0.07	12.2 ± 2.0	0.86 ± 0.02	15
60	0.22 ± 0.04	0.81 ± 0.11	0.78 ± 0.04	10.4 ± 0.9	0.63 ± 0.03	15
80	0.36 ± 0.05	0.45 ± 0.09	0.64 ± 0.05	5.3 ± 0.9	0.55 ± 0.02	16
100	0.48 ± 0.05	0.32 ± 0.04	0.52 ± 0.05	5.8 ± 1.1	0.51 ± 0.03	12
1 M KCl, 10 mM HEPES, pH 7.4						
20	—	—	—	—	1.00	4
40	—	—	—	—	0.09 ± 0.03	3
60	0.33 ± 0.12	0.48 ± 0.22	0.67 ± 0.12	4.0 ± 1.0	0.77 ± 0.05	4
80	0.40 ± 0.04	0.22 ± 0.05	0.60 ± 0.04	4.3 ± 2.2	0.63 ± 0.04	4
100	0.53 ± 0.03	0.23 ± 0.04	0.47 ± 0.03	4.9 ± 1.8	0.53 ± 0.02	4

voltage in the range of 40–80 mV (Fig. 11). At 40 mV the area of the conductance peak at 3.7 nS was fivefold larger than the peak at 1.6 nS, demonstrating the greater probability that the channel will occupy the maximal conductance state at low membrane voltages. When the membrane voltage was 80 mV, the relative probabilities for the channel residing in the either of the two states was reversed; finding the channel at 3.7 nS was half as likely as finding it at 1.6 nS. The ratio of 3.7/1.6 is 2.4, which is on the order of the twofold ratio determined by the voltage ramp data (Fig. 5) and the steady-state conductance–voltage plots (Fig. 6).

The mean values of the 3.7 and 1.6 nS were not significantly affected by voltage in the range of 20–100 mV. However, in addition to the two primary conductance states two substates were also evident in these histograms. A small shoulder present on the lower side of 3.7 nS peak in the 40-mV histogram was enlarged in the 60- and 80-mV histograms. This second peak was consistent with a less stable substate at ~3.1 nS. The apparently simple gaussian distribution around the 1.6 nS peak observed on

steps to 40 mV was altered at higher voltages and a conductance peak at 1.2 nS was evident.

The single-channel conductance histograms revealed that the channel behavior was more complex than the simple two-state model predicted from the multichannel conductance data. The two substates may result from minor changes in the channel conformations that determine the major conductance states. In this case, the value for G_{max} observed in the multichannel membrane is an average, weighted by the dwell times in 3.7 nS and the 3.1-nS substate. The value for G_{min} is the average of 1.6 nS and the 1.2 nS substate.

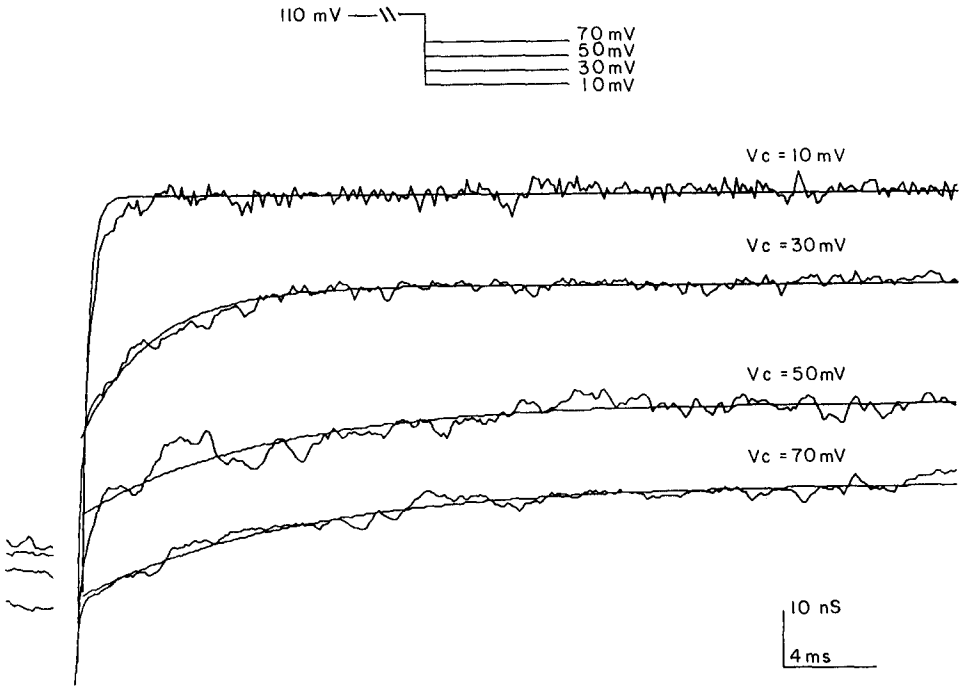

FIGURE 9. MIP channels open rapidly on return to low membrane voltages. The inset shows the voltage protocol applied; a 10-s prepulse to 110 mV was followed by a 40-ms test pulse to 70, 50, 30, or 10 mV. The data are plotted as conductance versus time. At the beginning of the records, the steady-state conductance reached during each 110 mV prepulse is shown; when the test voltage was applied a large mostly off-scale capacitive transient was followed by a conductance increase, which could be well fit by a single exponential. The time constants for the conductance increase were: 0.3 ms at 10 mV, 3.0 ms at 30 mV, 7.8 ms at 50 mV, and 9.8 ms at 70 mV.

Voltage dependence of first latencies. Records such as those shown in Fig. 10 were used to calculate the latency to first closing. This parameter was defined as time elapsing between the voltage step (V_h to V_c) and the channel closing from the 3.7- to the 1.6-nS conductance state. First latency histograms were measured for pulses to 40, 60, and 80 mV (Fig. 12). At all voltages the latency was well fit by a double exponential using the time constants derived during the fit of the relaxation data of the multichannel membranes (Table I). As with the multichannel kinetics, the rate of

closure increased with size of the voltage step. Thus, the latency to first closing paralleled the time course of current relaxations observed in membranes containing many channels.

Channel Modulation

Ionic strength. Current flow through the MIP channel was linearly proportional to the concentration of KCl over a 10-fold range of ionic strength. The *I-V* ramps in

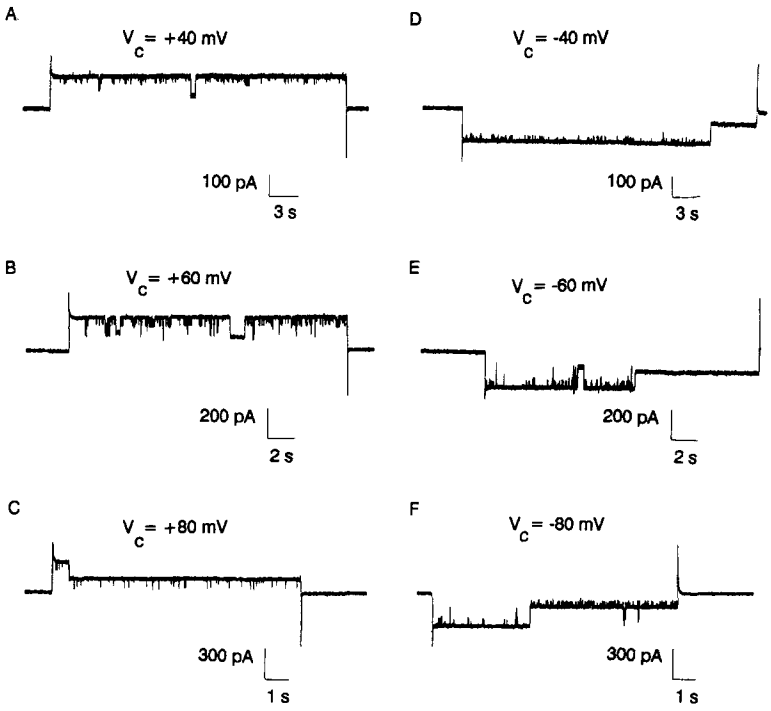

FIGURE 10. Currents through a single MIP channel in response to voltage pulses in 1 M KCl, pH 5.8. In all records, the holding potential (V_h) was 0 mV; the test pulse was marked by brief capacitive currents on the step to V_c and the return to V_h. Bars in each panel indicate the time and voltage scales. The single-channel currents demonstrate the same symmetry, with respect to the sign of V_c, as the multichannel currents shown in Fig. 7. For example, ~14 s after the step to 40 mV, the channel closed resulting in a decrease in the current from 150 to 65 pA; a similar channel closure (−151 to −70 pA) occurred at 17 s following the step to −40 mV. Pulses to ±60 and 80 mV also resulted in partial closures of the channel. In addition, to the two major conductance states brief channel transitions to possible substates are also seen in these records.

Fig. 13 show that the membrane currents through the channel were reduced approximately 5-fold in 0.2 M KCl or 10-fold in 0.1 M KCl with respect to the current in the 1.0 M KCl solution. The single-channel conductances for the most frequently observed conductance states were 3.5 and 1.6 nS in 1 M KCl, 0.73 and 0.36 in 0.2 M KCl, and 0.38 and 0.18 nS in 0.1 M KCl. These data suggest that there is little interaction between these ions within the channel.

In the lower ionic strength solutions, the channel occasionally closed from its maximally open state to a conductance approximating that of the bare bilayer (Fig. 14). These closures, while infrequent (<1% of the total number of closures observed), demonstrate that conditions exist in which the reconstituted MIP channel can close completely. If MIP functions as a channel in cell membranes, the fully closed state must be more prevalent *in vivo* than observed in our reconstitutions.

Selectivity. The channel was slightly anion selective as determined from reversal potentials of single-channel currents (Fig. 15) When the membrane was bathed with 1.0 M KCl in both the front and rear compartments the reversal potential was near 0 mV. Substitution of the solution in the rear compartment with 0.1 M KCl resulted in a reversal potential of −16 mV. With the configuration of the bilayer setup used in this experiment (virtual ground in the front chamber) this shift indicates that the

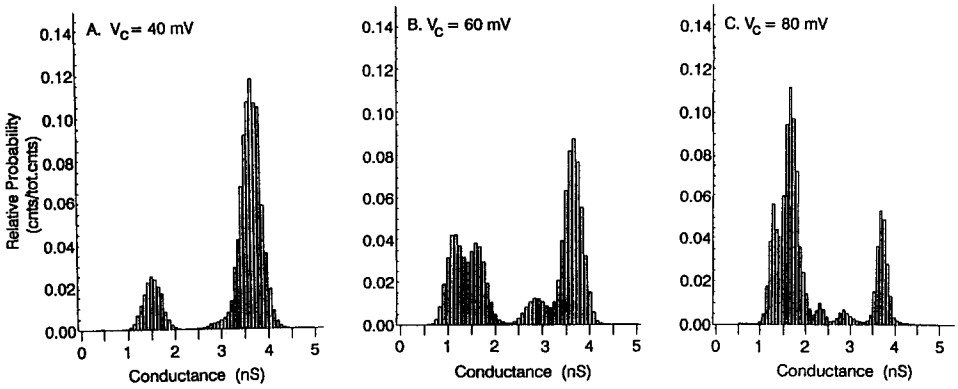

FIGURE 11. Conductance histograms were calculated from records similar to those shown in Fig. 10. Five pulses each to 40, 60, and 80 mV were analyzed. Bin sizes were 0.075 nS for *A* and *C* and 0.083 nS for *B*. In the 40-mV histogram, two conductance states are evident with gaussian distributions around 3.7 and 1.6 nS. The probability of the channel occupying 3.7-nS conductance state was fivefold that of it occupying the 1.6-nS state at 40 mV. As the voltage was increased to 60 and 80 mV the probability that channel would occupy the 3.7-nS state was reduced and the probability that it would occupy 1.6 nS state was increased. In addition, to the main conductance states, subconductance states are also evident in the 60- and 80-mV histograms.

channel possesses a slight anionic selectivity. In five similar experiments using *I-V* ramps the mean shift in the reversal potential was −11.4 ± 3 mV for a 10-fold difference in KCl concentration across the membrane, making the ratio of P_{Cl}/P_K slightly less than 1.8. Thus there appears to be a slight, but significant ($P < 0.002$) selectivity for chloride over postassium as the charge carrier through the channel.

Changes in pH. Analyses of continuous *I-V* ramps and single-channel recordings (data not shown) demonstrated that the single-channel conductance remained constant as the pH of the solution was altered from 5.8 to 7.4. However, changes in pH over this range had a small effect on the voltage-dependence of the channels. At most voltages, the values for steady-state conductance in multichannel membranes obtained at pH 7.4 were not significantly different ($P > 0.05$) from those measured at pH 5.7 (Fig. 16; Table I). At pH 7.4, however, there was a slight but significant

decrease in the effect of voltage on the conductance near the midpoint of the conductance–voltage curve. For example, when the membrane was held to 60 mV, the steady-state conductance was reduced to 0.77 ± 0.05 at pH 7.4 and to 0.63 ± 0.03 at pH 5.8 ($P < 0.05$). A least squares fit of the Boltzmann distribution to the data obtained at pH 7.4 showed no significant change in the values for the ratio of

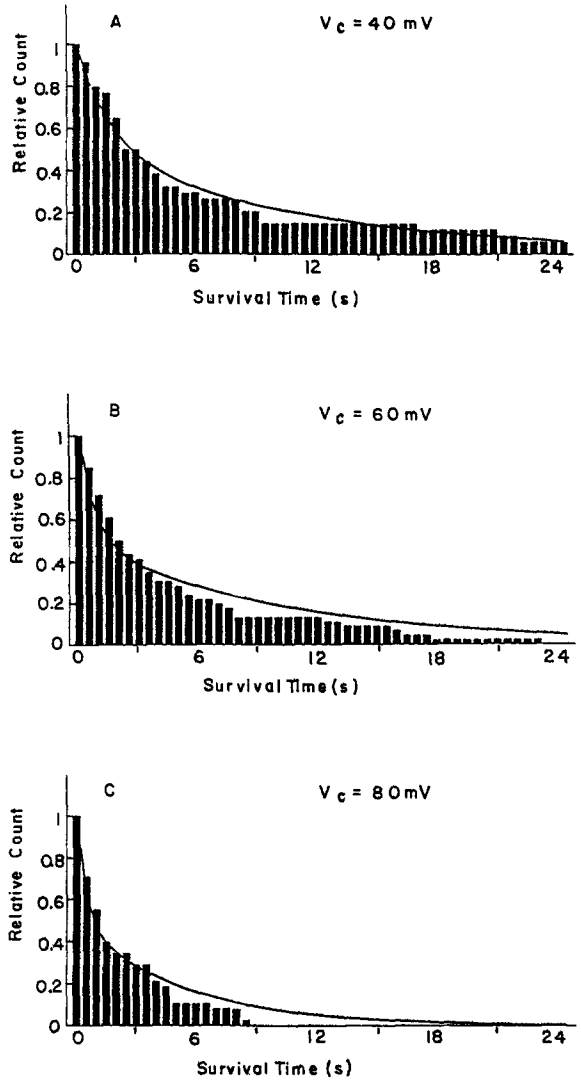

FIGURE 12. The latencies to first channel closure after a voltage step were measured from 30 sets of records such as those shown in Fig. 10. The histograms plot the fraction of channels remaining open against the time after voltage steps to 40, 60, or 80 mV. The latency to first closing is decreased with increases in V_c. The solid line represents the expected distribution of closings using time constants derived in multi-channel kinetic experiments (Figs. 6 and 7; Table I). Note that the single-channel latency distributions are well fit by this double exponential time course.

G_{min}/G_{max}, V_0, or the apparent gating charge for the channel. Moreover, pH had only a marginal effect on the kinetics of channel closing (Table I). At pH 7.4, time constants measured for the fast (I_f) components of the current were not significantly different from those measured at pH 5.8. For the slow component of the current (I_s), only the time constant measured at 60 mV was affected by changes in pH from

5.8 to 7.4 (Table I). In sum, these effects were relatively minor, but at the acid pH the effect of voltage on the channel was slightly augmented.

Changes in pCa. Changing calcium concentration in the bathing solution from 10^{-7} to 10^{-2} M had no effect on the single-channel conductance or the voltage dependence of the channel as determined by continuous *I-V* ramps.

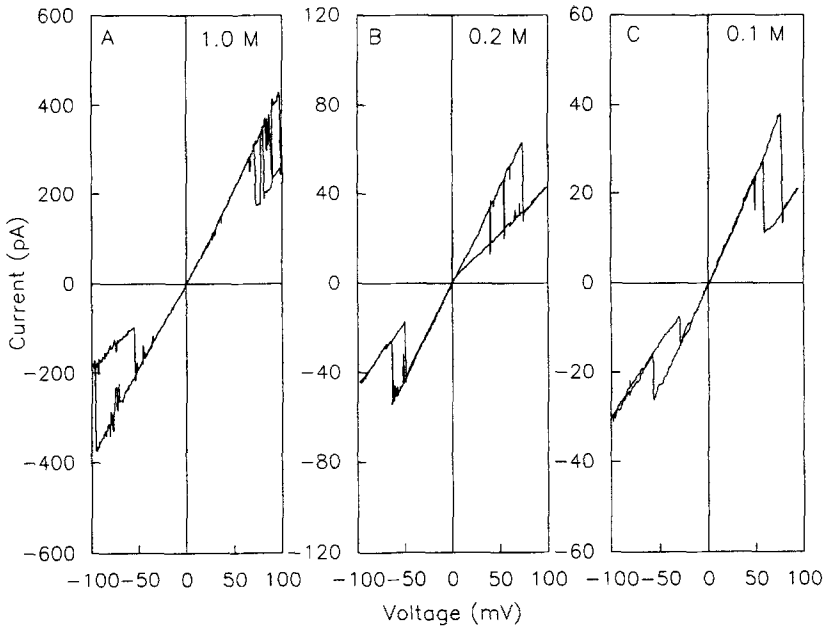

FIGURE 13. The effects of changes in ionic strength on single-channel conductance were measured using voltage ramps. Symmetric solutions of 1.0, 0.2, or 0.1 M KCl were used. Note that the current scales for each of the three panels have been adjusted to compensate for alterations in the ionic strength of the bath solution. The slope of the *I-V* curve at 0 mV (the maximum conductance during the ramps) was a linear function of ionic strength over a 10-fold change in the concentration of KCl. In addition, the minimum conductance measured during these ramps was a linear function of ionic strength.

DISCUSSION

Does MIP Actually Form the Reconstituted Channel?

Identification of the molecules responsible for the electrical events recorded in bilayers is essential in reconstitution studies. This identification is difficult for MIP because of the lack of specific reagents that affect the channel.

In this study, purified MIP reconstituted into planar bilayers produced channels which were virtually indistinguishable in voltage dependence, single-channel conductance, and multichannel kinetics from channels obtained using solubilized protein from adult bovine or calf lens plasma membranes. In a previous publication, we constructed a statistical argument that the protein responsible for the observed channels must have comprised at least 20% of the protein in the lens membrane isolate (Zampighi et al., 1985; Ehring et al., 1988). This eliminated the possibility that

the channel was due to a trace contaminant and identified three possible candidates for the channel-forming protein (MIP, a 22-kD band, and a 16-kD band). The additional data available from the HPLC purified material now make the statistical argument somewhat stronger. If we call p the probability that a vesicle contains at least one MIP channel, ν the number of vesicles that adhere to the planar membrane, n the number of experiments in which no channels were observed, and m the number of channels in which at least one channel was observed, we can calculate p from the formula:

$$p = 1 - [n/(m + n)]^{1/\nu}.$$

Under the conditions used for our experiments, direct observation of fluorescently labeled vesicles indicated that about 20–50 vesicles adhere to the membrane (Zampighi et al., 1985). For HPLC-purified material we found an n of 3 and an m of 55. Taking ν as ranging from 50 to 20 gives a range from 0.60 to 0.14 for p. This

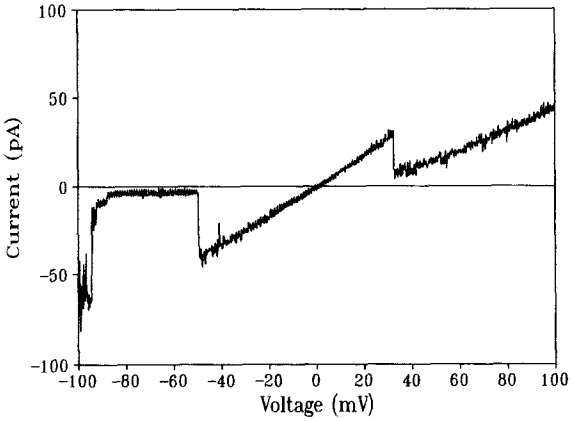

FIGURE 14. Complete channel closure in symmetric 200 mM KCl. Single-channel *I-V* ramps showed channel transitions between the 370-pS conductance state and the bare bilayer conductance. The membrane was held at 0 mV between ramps. V_c was stepped to −100 mV and then ramped to +100 mV at a rate of 10 mV/s. When V_c reached 95 mV, the current decreased in steps to the bare bilayer level. The channel then opened to its original conductance at 50 mV. Such closures were observed only rarely. In the low ionic strength solutions, <1% of the channel transitions were complete closures.

means 6–14 of every 100 vesicles must contain the channel-forming protein. Thus the worst possible case is that at least 6% of the protein reconstituted into the vesicles is the channel-forming protein. A protein which constituted one percent of the total HPLC-purified material would have given a distinct band on the silver-stained SDS gels. No such band, other than that where MIP runs was observed. Thus unless our estimate of the number of adhering vesicles is much too low, MIP (or possibly another protein which co-purifies with MIP on HPLC and runs the same on SDS-PAGE) must be the channel-forming protein.

What Is the Structure of the Channel?

MIP is a membrane-spanning protein. When MIP is reconstituted into unilamellar vesicles it forms distinct particles on the vesicle fracture faces. The number of particles observed is directly related to protein/lipid ratio used during reconstitution.

This result is direct evidence that MIP is a membrane-spanning protein. Indirect eivdence that MIP is a membrane-spanning protein is found in a structural model calculated from its deduced amino acid sequence (Gorin et al., 1984). MIP is depicted as having six membrane-spanning domains and having both its carboxy and amino termini on the cytoplasmic side of the membrane. At least one of the membrane-spanning domains is amphipathic and could contribute to the formation of a hydrophillic pore. Additional evidence that MIP is a membrane spanning protein is derived from secondary and tertiary structure of MIP as determined by near and far ultraviolet circular dichroism (Girsch and Peracchia, 1985*b*; Horwitz and Bok, 1987). In studies of both octyl β-D-glucopyranoside-solubilized MIP and a detergent-free membrane preparation enriched for MIP, Horwitz and Bok (1987) determined that the structure of MIP consists of ~50% α-helix and 20% β-sheet. Such a model for MIP is consistent with models for other channel-forming proteins, for example, alamethecin (Hall et al., 1984), the sodium channel (Noda and Numa, 1987), the acetylcholine channel (Stroud, 1987), and the liver gap junction channel (Paul, 1986; Gilula, 1987; Zimmer et al., 1987; Goodenough et al., 1988).

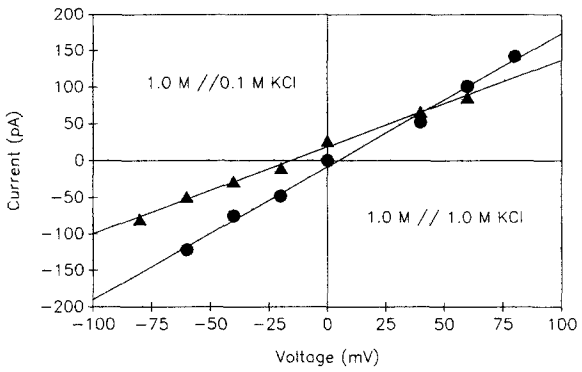

FIGURE 15. Anion selectivity of MIP channels. Single-channel currents were measured with either 1.0 M KCl in both compartments of the bilayer chamber (●) or with 1.0 M KCl in the front compartment and 0.1 M KCl in the rear compartment (▲). The solid lines show the best fit linear regressions for the currents; R^2 was 0.97 for both curves. The reversal potential for the current (measured as size of the current steps at each V_c) was 0 mV in the symmetric KCl solutions. When the rear chamber was perfused with 0.1 M KCl the reversal potential was −16 mV suggesting a slight anionic selectivity of the channel.

MIP channels are tetramers. The number of polypeptides composing the channel is usually uncertain because very few methods can determine this number in solution or in bilayers. Proteins that exist at high concentration in the membrane, however, can be crystallized and the number of polypeptides forming the channel can be unequivocally determined with knowledge of the molecular weight of the polypeptide, the unit cell dimensions and the plane group symmetry. Antibody staining in label-fracture replicas of isolated lens membrane (Zampighi et al., 1989) has demonstrated tetragonal arrays composed of MIP. In addition x-ray diffraction studies of partially oriented lens plasma membranes show sharp equatorial reflections that index in a tetragonal lattice (Simon et al., 1982; Zampighi et al., 1982; Costello et al., 1989). Tetragonal arrays with a 6–7 nm unit cell have been seen in lens fibers (Okinami, 1978; Peracchia, 1978; Peracchia and Peracchia, 1980*a*, *b*; Bernardini and Peracchia, 1981; Simon et al., 1982; Costello et al., 1985).

Reconstitution into unilamellar liposomes requires that the membranes be solubilized with detergent, a treatment which could disrupt the tetramers. Change in aggregation number upon solubilization has been reported for other membrane proteins such as bacteriorhodopsin (Michel et al., 1980; Glaeser et al., 1985) and cytochrome oxidase (Fuller et al., 1979). Therefore, one cannot assume MIP forms tetramers after solubilization and reconstitution simply because it appears to be organized as a tetramer in the cell.

However, when the protein was reconstituted at a protein-to-lipid ratio of 1:100 instead of the usual 1:1,000 or 1:10,000 required for the electrical studies, crystalline patches appeared. As noted earlier, these crystals had tetragonal symmetry and a unit cell volume of 283–305 nm^3 (6.6 × 6.6 × 6.5–7.0 nm). This range of unit cell volumes can accommodate four MIP molecules and associated lipid. It thus seems likely that the channels we observe are formed by tetramers of MIP.

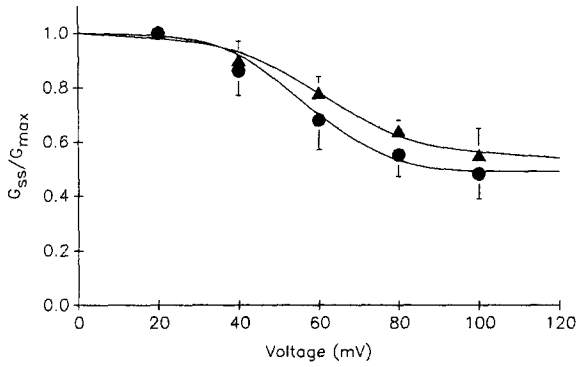

FIGURE 16. Comparison of the conductance-voltage relationship in 1 M KCl, pH 5.8 vs. 1 M KCl, pH 7.4 solutions. The mean and standard error of the normalized steady-state conductances were calculated as described in Fig. 5 and plotted against membrane voltage. Circles summarize data from 15 experiments done at pH 5.8. Triangles show the results from five experiments done at pH 7.4. Solid lines represent least squares regression of a two-state Boltzmann model for the channel. At pH 7.4 the best fit parameters were $G_{min}/G_{max} = 0.54 \pm .08$, $n = 2.01 \pm 0.60$ *e* and $V_0 = 61 \pm 6$ mV. At pH 5.8 they were $G_{min}/G_{max} = 0.49 \pm .08$, $n = 2.61 \pm 0.57$ *e* and $V_0 = 57 \pm 9$ mV.

Channel Properties

The principal features of the reconstituted MIP channel are large single-channel conductance, limited anionic selectivity, symmetrical voltage dependence, rapid opening and slow closing rates, and insensitivity to Ca^+ and H^+ ion concentration.

Direct comparison of the MIP channel to an in vivo channel is not possible becasue of a lack of electrophysiological studies on isolated lens fibers. However, Rae and co-workers have observed a large channel (γ = 380–440 pS in physiological salt solutions) during patch clamp experiments on lens epithelial cells (Rae and Levis, 1984; Rae, 1985). This nonselective channel has a voltage dependence similar to that of the MIP channel.

Preliminary state diagram. Our data do not allow the construction of a detailed kinetic model, but conductance data, principally single-channnel conductance histograms, and kinetic data taken together suggest a preliminary state diagram.

The channel has four conductance states in 1 M KCl, two high-conductance states (3.7 and 3.1 nS) and two low-conductance states (1.6 and 1.2 nS). Single-channel

probability histograms show that the channel spends most of its time in the high conductance states at low voltages and in the low conductance states at high voltage. Because the voltage dependence of many channel membranes is well-fit by a two-state Boltzmann distribution, the pair of high-conductance states approximate a single high-conductance state, and the pair of low-conductance states approximate a single low-conductance state.

Modeling the high-conductance pair as one state fits the steady-state voltage dependence but fails to descibe the kinetics of closure. The presence of two exponentials in both the multichannel current relaxation (Fig. 7) and single-channel first latency experiments (Fig. 12) demands that closure take place from two or more high-conductance states (Colquhoun and Hawkes, 1983).

By contrast the presence of only a single exponential in the rapid increase in conduction from G_{min} to G_{max} implies that the channel opens from a single conductance state. While the data on opening kinetics cover a much smaller temporal range than the channel closing experiments, this hypothesis is also supported by the observation that in single-channel membranes the channel opens to the higher conductance states from the 1.6-nS state, but not the 1.2-nS state. The two low-conductance states are thus nearly equivalent for modeling both steady state voltage dependence and kinetics.

We summarize these observations in the following state diagram:

$$\begin{array}{ccc} H_{3.7} & \rightleftharpoons & L_{1.6} \\ \uparrow\downarrow & \not\nearrow & \downarrow\uparrow \\ H_{3.1} & & L_{1.2} \end{array}$$

H and L denote the high and low conductance states, equivalent for purposes of steady-state voltage dependence. The subscripts denote the conductance of each state in 1 M KCl in nanosiemens.

Physiological Significance

The properties of the reconstituted channel taken together with the immunocytochemical localization of MIP in lens plasma membranes suggest a possible role of the MIP channel in lens physiology. The most important property of the lens is transparency. Transparency is much reduced by light scattering if the index of refraction of the lens varies on a spatial scale greater than about a quarter wavelength of visible light (Benedek, 1971). The index of refraction of extracellular fluid is lower than that of cytoplasm owing to the presence in the cytoplasm of a very high concentration of crystalline proteins (Bettelheim, 1985). Thus, the presence of pockets of extracellular space with dimensions >100–200 nm would severely reduce the transparency of the lens.

We believe that a channel with the properties of the reconstituted MIP channel could play an important role in maintaining fluid balance and minimizing extracellular space in the lens. Because of the negative charge on the impermeant intracellcular protein, Gibbs-Donnan equilibrium dictates that in the presence of an open MIP channel, ions of both signs would flow into the cell followed by water. The concentration of fixed negative charges in the mammalian lens is about 100 mM (Duncan and Croghan, 1989). This means the concentration of sodium in the lens, should it be allowed to reach its equilibrium, would approach 140 mM.

The MIP channel has a very large conductance and if it were open in the plasma membrane of lens cells bathed in unrestricted extracellular space, it would allow sodium to move into the cell down its electrochemical gradient. Chloride would rush in along with the sodium and this would cause the cell to lyse through colloid osmotic swelling. However, in the lens nucleus, the extracellular space is only 0.7 nm in width (Zampighi et al., 1989). The narrowness of this space would result in a very large resistance to the flow of both ions and fluid from extracellular space. This large resistance could in fact be the major limitation on the rate that ions and fluid could enter the fibers even through a very large conductance channel. If this were the case, an open MIP channel deep in the lens would not promote colloid osmotic lysis, but would serve to minimize extracellular space by promoting uptake of sodium into the fibers deep in the nucleus of the lens. For osmotic balance to be maintained, this sodium would eventually have to be pumped out of the fiber cells. Presumably it would pass from the cytoplasm of the fiber cells to the cytoplasm of the anterior epithelial cells via gap junctions and then be pumped out by the NaK-ATPase of the anterior epithelial cells.

We propose that an MIP channel open in the interior of the lens would be beneficial, while one open near the surface of the lens might do damage by causing lysis. If there are MIP channels in the lens with the same voltage dependence as the reconstituted channels described above, the gradient of membrane potentials from the cortex to the nucleus of the lens described by Mathias and Rae (1985) would result in these channels being closed near the periphery of the lens and open in the nuclear region. Fig. 17*A* shows a plot of extracellular and intracellular voltage in the frog lens as measured by Mathias and Rae; the voltage drop across the cell membranes decreases toward the center of the lens. Using their measured voltage drops and using the voltage dependence of the steady-state conductance in our Fig. 6, we can calculate the probability that the MIP channel is open as a function of position in the lens (Fig. 17 *B*). Note that the probability of the MIP channel being open rises sharply going from the exterior to the interior and plateaus near the cortex–nucleus boundary.

Moreover, the geometry of the spaces between the fiber cells of the lens nucleus is such that channels having properties like those we have measured for the reconstituted MIP channel could contribute substantially to cell–cell coupling (Heppner, and Plonsey, 1970; Bennett, 1977). The space between the cells is essentially two dimensional, the membranes being separated by ~0.7 nm. Thus, the conductance of the intermembrane space connecting a channel in one membrane with a channel some distance away in the other membrane is given by

$$G = \pi d/[\rho \ln (h/a)],$$

where h is the distance separating the channels, d is the distance separating the bilayers, ρ is the resistivity of the extracellular fluid, and a the radius of the pore.[2]

The cell-to-cell conductance via the extracellular space thus becomes

$$G = 1/[(2/\gamma) + [\rho \ln (h/a)]/(\pi d)]],$$

[2]The problem can be easily solved by realizing that it is the same as calculating the resistance per unit length between two long straight wires of diameter a and separation h. Methods for solving this problem can be found in any standard electrostatics text; for example, see Benumof (1961).

where γ is the single-channel conductance of the channel in one membrane. When h equals a, the cell-to-cell conductance becomes $\gamma/2$. If we assume that ρ is on the order of 100 Ω-cm, a is on the order of 0.6 nm, and d on the order of 0.7 nm, then the cell-to-cell conductance only drops to about 80% of its maximum when the channels are separated by 200 channel diameters. Although MIP may not form a gap junction, it may contribute substantially to the coupling of the lens and thus masquerade as a gap junctional channel, especially in the center of the lens.

There are several difficulties with this view of the MIP channel. First, the reconstituted channel did not close completely in 1 M KCl. This is important for our

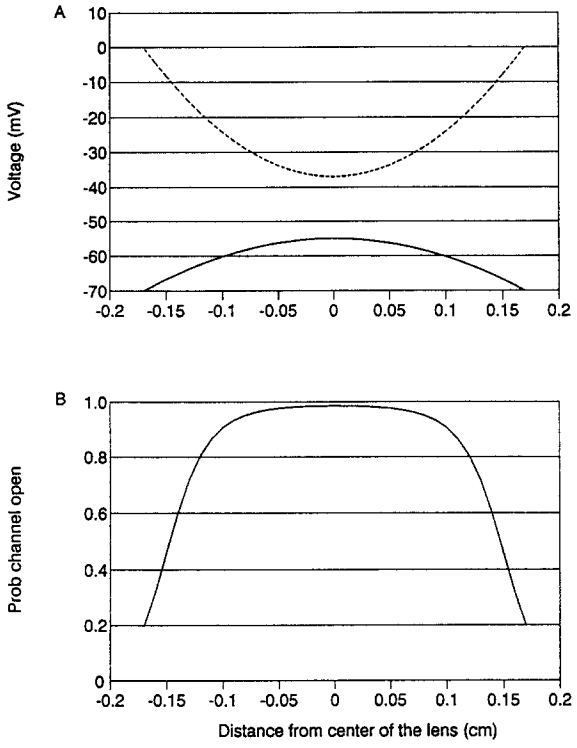

FIGURE 17. Calculated distribution of open MIP channels in the lens. (*A*) The positional dependence of both extracellular voltage (*dotted line*) and intercellular voltage (*solid line*) replotted from data of Mathias and Rae (1985). Note that the voltage drop across the cell membranes decreases from about 70 mV near the periphery of the lens to only bout 20 mV at the center. (*B*) Probability that a channel having the voltage dependence we measured for the reconstituted MIP channel would be in the open state plotted on the same spatial scale as the voltages shown in *A*. The probability that the channel is open is near zero at the periphery of the lens and reaches 0.9 a distance of 1 mm from the center of the lens, the approximate position of the boundary between the nucleus and the cortex. Channels reconstituted in lipid bilayers usually close only partially high voltages, but in 200 mM salt they occasionally close completely. We thus believe it is possible that the channels close completely in vivo.

model, since even the minimum open conductance state is large enough to pose a serious osmotic threat to a cell. Thus for our view to be correct, the channel must be capable of closing completely. Fig. 14 shows that the channel can close completely in 200 mM salt. Although complete channel closures were rare events, there may be several other factors which promote complete closure. In bilayer experiments, a component of serum can transiently reduce the conductance of the MIP channel to near zero (Ehring et al., 1988). Additional cytoplasmic regulators may be present in the lens and these could provide a mechanism for controlling fluid balance in the lens by adjusting the permeability of lens fibers.

The second difficulty is that no channel with exactly the properties of the MIP channel has been found in lens tissue. The large nonselective channel seen by Rae and co-workers comes closest, and may represent an MIP channel modified by cytoplasmic factors not present in our bilayer experiments. But Rae (1985) did not see MIP-like channels in cell-attached patches made on fiber cells near the lens nucleus, and the impedance studies have demonstrated that the membranes of fiber cells are best modeled as having a very large specific resistance, on the order of 1 $m\Omega\text{-}cm^2$ (Mathias et al., 1979; Mathias et al., 1981). If even a small fraction of the MIP in the lens nucleus formed channels whose primary contribution was to the membrane conductance, the value of membrane conductance measured by Mathias and Rae should have been much higher. We believe this was not the case because, while the channels formed by MIP are not morphologically gap junction channels, they are functionally very similar to gap junctions. Plaques containing a high density of MIP channels would tend to contribute to cell-to-cell conductance in proportion to the area of the plaque, and to cytoplasm-to-extracellular space conductance in proportion to the circumference of the plaque. Thus sufficiently large plaques would make a large contribution to cell-to-cell conductance but virtually none to cytoplasm-to-extracellular space conductance. MIP channels would thus show up in the impedance measurements of Mathias and Rae as part of the parameter describing cell coupling (which indicates a very low resistance) rather than the parameter describing cytoplasm-to-extracellular resistance (which indicates a very high resistance).

The fact that Rae (1985) did not observe MIP channels in fiber cells poses a problem for our model. It is possible channels were not observed because MIP does not form a channel *in situ*. However, as pointed out by Rae there are several other possibilities that could explain the absence of channels in his cell-attached patches. First, the large specific resistance of the lens fiber membrane exposed to unrestricted extracellular space predicts that an open MIP channel may be an extremely rare event. Since cell-attached patch configuration detects channels in the $\sim 1\ \mu m^2$ directly under electrode tip, it is possible that channels were in areas of the membrane not sampled. Secondly, the cell-attached patch configuration detects channels that are opening and closing. At low voltages (<40 mV) transitions between the high conductances state to the low conductance states are very rare and conversely at high voltages (>100 mV) transitions from the low-conductance to high-conductance states are rare. Thus, it is possible that the voltage protocol used by Rae in his experiments precluded the observation of MIP channels. Thirdly, the dissection necessary to expose deep fibers may have brought into play cytoplasmic factors tending to close MIP channels. Fourthly, the junctional structures formed by MIP could have been disrupted by the dissection required to access the deep fiber cells. Our model predicts that MIP functions as a channel within these specialized junctional regions. At present, this view is not supported directly by any experimental data from the lens. However, it does suggest potential role for a channel with similar properties to the reconstituted MIP channel and is consistent with its immunocytochemical localization in the lens. It is very difficult to study the macroscopic electrophysiological properties of nuclear fiber cells, but this difficulty must be overcome if the view of the MIP channel presented above is to be ruled out or supported.

Whether or not MIP forms gap junctions has been a controversial question for some time. Some authors have contended that MIP forms true gap junctions (Benedetti et al., 1976; Gorin et al., 1984; Johnson et al., 1985), while others have argued that MIP is a structural protein (Costello et al., 1989; Gruijters, 1989). Though clearly unproven, our hypothesis reconciles these views, first by providing a role for MIP in fiber cell communication and second by showing how cell-to-cell communication can be mediated even without the requirement that MIP form proper gap junctions. Our view that MIP facilitates the osmotically driven collapse of extracellular space provides a role for MIP consistent with existing data and the functions of the lens.

The authors are grateful to Drs. David Paul and Dan Goodenough for supplying us with the antibody to MIP and to Dr. Joerg Kistler for supplying us with the antibody to MP 70. We thank Ms. Mary Hawley and Mr. Mike Kreman for their excellent technical assistance.

This work was supported by National Institutes of Health grants EY-06075, EY-05661, and EY-04110.

Original version received 31 July 1989 and accepted version received 10 April 1990.

REFERENCES

Benedek, G. B. 1971. Theory of transparency of the eye. *Applied Optics.* 10:459–473.

Benedetti, E. L., I. Dunia, C. J. Bentzel, A. J. M. Vermorken, M. Kibbelaar, and H. Bloemendal. 1976. A portrait of plasma membrane specializations in eye lens epithelium fibers. *Biochimica et Biophysica Acta.* 457:353–384.

Bennett, M. V. L. 1977. Electrical transmission: a functional analysis and comparison to chemical transmission. *Handbook of Physiology.* Sec. I, Vol. I. 357–416.

Benumof, R. 1961. Concepts in Electricity and Magnetism. Holt, Rinehart and Winston, New York. 1–374.

Bernardini, G., and C. Peracchia. 1981. Gap junction crystallization in lens fibers after an increase in cell calcium. *Investigative Ophthalmology and Visual Science.* 21:291–299.

Bettelheim, F. A. 1985. Physical basis of lens transparency. *In* The Ocular Lens: Structure, Function and Pathology. H. Maisel, editor. Marcel Dekker, Inc., New York. 265–300.

Bevington, P. R. 1969. Least-squares fit to an arbitrary function. *In* Data Reduction and Error Analysis for the Physical Sciences. McGraw Hill, Inc., New York. 204–246.

Bok, D., J. Dockstader, and J. Horwitz. 1982. Immunocytochemical localization of the lens main intrinsic polypeptide (MIP) in communicating junctions. *Journal of Cell Biology.* 92:213–220.

Burnette, W. N. 1981. "Western blotting": electrophoretic transfer of proteins from sodium dodecyl sulfate-polyacrylamide gels to unmodified nitrocellulose and radiographic detection with antibody and radioiodinated protein A. *Analytical Biochemistry.* 112:193–203.

Colquhoun, D., and A. G. Hawkes. 1983. The principles of the stochastic interpretation of ion-channel mechanisms. *In* Single-Channel Recording. B. Sakmann and E. Neher, editors. Plenum Press, New York. 135–175.

Costello, M. J., T. J. McIntosh, and J. D. Robertson. 1985. Membrane specializations in mammalian lens fiber cells: distribution of square arrays. *Current Eye Research.* 4:1183–1201.

Costello, M. J., T. J. McIntosh, and J. D. Robertson. 1989. Distribution of gap junctions and square array junctions in the mammalian lens. *Investigative Ophthalmology and Visual Science.* 30:975–989.

Dahl, G., T. M. Miller, D. L. Paul, R. Voellmy, and R. Werner. 1987. Expression of functional cell-cell channels from cloned rat liver gap junction complementary DNA. *Science.* 236:1290–1293.

Dickson, D. H., and G. W. Crock. 1972. Interlocking patterns on primate lens fibers. *Investigative Ophthalmology.* 11:809–815.

Duncan, G., and P. C. Croghan. 1989. Mechanisms for the regulation of cell volume with particular reference to the lens. *Experimental Eye Research.* 8:421–430.

Ebihara, L., E. C. Beyer, K. I. Swenson, D. L. Paul, and D. A. Goodenough. 1989. Cloning and expression of a *Xenopus* embryonic gap junction protein. *Science.* 243:1194–1195.

Ehring, G. R., and J. E. Hall. 1988. Single channel properties of lens MIP 28 reconstituted into planar lipid bilayers. *Proceedings of the Western Pharmacology Society.* 31:251–253.

Ehring, G. R., and J. E. Hall. 1989. Reconstitution of junctional channels from lens. *In* Cell Interactions and Gap Junctions: Volume I. N. Sperelakis and W. C. Cole, editors. CRC Press, Boca Raton, FL. 51–58.

Ehring, G. R., G. A. Zampighi, and J. E. Hall. 1988. Properties of MIP 26 channels reconstituted into planar lipid bilayers. *In* Gap Junctions. R. G. Johnson and E. L. Hertzberg, editors. Alan R. Liss, Inc., New York. 335–346.

Fitzgerald, P. G., D. Bok, and J. Horwitz. 1983. Immunocytological localization of the main intrinsic polypeptide (MIP) in ultrathin frozen sections of rat lens. *Journal of Cell Biology.* 97:1491–1499.

Fitzgerald, P. G., D. Bok, and J. Horwitz. 1985. The distribution of the main intrinsic membrane polypeptide in ocular lens. *Current Eye Research.* 4:1203–1217.

Fuller, S. D., R. A. Capaldi, and R. Henderson. 1979. Structure of cytochrome c oxidase in deoxycholate-drived two-dimensional crystals. *Journal of Molecular Biology.* 134:305–327.

Gilula, N. B. 1987. Topology of gap junction protein and channel function. *Ciba Foundation Symposium.* 125:128–139.

Girsch, S. J., and C. Peracchia. 1985*a*. Lens cell-to-cell channel protein. I. Self-assembly into liposomes and permeability regulation by calmodulin. *Journal of Membrane Biology.* 83:217–225.

Girsch, S. J., and C. Peracchia. 1985*b*. Lens cell-to-cell channel protein. II. Conformational change in the presence of calmodulin. *Journal of Membrane Biology.* 83:227–233.

Glaeser, R. M., J. S. Jubb, and R. Henderson. 1985. Structural comparison of native and deoxycholate-treated purple membrane. *Biophysical Journal.* 48:775–780.

Gooden, M. M., D. A. Rintoul, M. Takehana, and L. J. Takemoto. 1985*a*. Major intrinsic polypeptide (MIP26K) from lens membrane: reconstitution into vesicles and inhibition of channel forming activity by peptide antiserum. *Biochemical and Biophysical Research Communications.* 128:993–999.

Gooden, M. M., L. J. Takemoto, and D. A. Rintoul. 1985*b*. Reconstitution of MIP26 from single human lenses into artificial membranes. I. Differences in pH sensitivity of cataractous vs. normal human lens fiber cell proteins. *Current Eye Research.* 4:1107–1115.

Goodenough, D. A., D. L. Paul, and L. Jesaitis. 1988. Topological distribution of two connexin32 antigenic sites in intact and split rodent hepatocyte gap junctions. *Journal of Cell Biology.* 107:1817–1824.

Gorin, M. B., S. B. Yancey, J. Cline, J. P. Revel, and J. Horwitz. 1984. The major intrinsic protein (MIP) of the bovine lens fiber membrane: characterization and structure based on cDNA cloning. *Cell.* 39:49–59.

Gruijters, W. T., J. Kistler, S. Bullivant, and D. A. Goodenough. 1987. Immunolocalization of MP70 in lens fiber 16–17-nm intercellular junctions. *Journal of Cell Biology.* 104:565–572.

Gruijters, W. T. M. 1989. A non-connexon protein (MIP) is involved in eye lens gap-junction formation. *Journal of Cell Science.* 93:509–513.

Hall, J. E., I. Vodyanoy, T. M. Balasubramanian, and G. R. Marshall. 1984. Alamethicin: a rich model for channel behavior. *Biophysical Journal.* 45:233–247.

Heppner, D. B., and R. Plonsey. 1970. Simulation of electrical interaction of cardiac cells. *Biophysical Journal.* 11:1057–1075.

Hertzberg, E. L., D. J. Anderson, M. Friedlander, and N. B. Gilula. 1982. Comparative analysis of the major polypeptides from liver gap junctions and lens fiber junctions. *Journal of Cell Biology.* 92:53–59.

Horwitz, J., and D. Bok. 1987. Conformational properties of the main intrinsic polypeptide (MIP26) isolated from lens plasma membranes. *Biochemistry.* 26:8092–8098.

Johnson, R., E. Frenzel, K. Johnson, K. Klukas, P. Lampe, D. Sas, R. Biegon, and C. Louis. 1985. Is lens MP26 a gap junction protein? A phosphoprotein? *In* Gap Junctions. M. V. L. Bennett and D. C. Spray, editors. Cold Spring Harbor Laboratory, Cold Spring Harbor, NY. 91–105.

Kistler, J., B. Kirkland, and S. Bullivant. 1985. Identification of a 70,000-D protein in lens membrane junctional domains. *Journal of Cell Biology.* 101:28–35.

Kistler, J., D. Christie, and S. Bullivant. 1988. Homologies between gap junction proteins in lens, heart and liver. *Nature.* 721–773.

Kumar, N. M., and N. B. Gilula. 1986. Cloning and characterization of human and rat liver cDNAs coding for a gap junction protein. *Journal of Cell Biology.* 103:767–776.

Kuwabara, T. 1975. The maturation of the lens cell: a morphologic study. *Experimental Eye Research.* 20:427–433.

Laemmli, U. K. 1970. Cleavage of structural proteins during the assembly of the head of bacteriophage T4. *Nature.* 227:680–685.

Lowry, O., N. Rosebrough, A. Farr, and R. Randall. 1951. Protein measurement with the Folin phenol reagent. *Journal of Biological Chemistry.* 193:265–275.

Mathias, R. T., J. L. Rae, and R. S. Eisenberg. 1979. Electrical properties of structural components of the crystalline lens. *Biophysical Journal.* 25:181–201.

Mathias, R. T., J. L. Rae, and R. S. Eisenberg. 1981. The lens as a nonuniform spherical syncytium. *Biophysical Journal.* 34:61–83.

Mathias, R. T., and J. L. Rae. 1985. Steady state voltages in the frog lens. *Current Eye Research.* 4:421–430.

Michel, H., D. Oesterhelt, and R. Henderson. 1980. Orthorhombic two-dimensional crystal form of purple membrane. *Proceedings of the National Academy of Sciences of the United States of America.* 77:338–342.

Miller, T. M., and D. A. Goodenough. 1986. Evidence for two physiologically distinct gap junctions expressed by the chick lens epithelial cell. *Journal of Cell Biology.* 102:194–199.

Montal, M., and P. Mueller. 1972. Formation of bimolecular membranes from lipid monolayers and a study of their electrical properties. *Proceedings of the National Academy of Sciences of the United States of America.* 69:3561–3566.

Nicholson, B. J., L. J. Takemoto, M. W. Hunkapiller, L. E. Hood, and J. P. Revel. 1983. Differences between liver gap junction protein and lens MIP 26 from rat: implications for tissue specificity of gap junctions. *Cell.* 32:967–978.

Nikaido, H., and E. Y. Rosenberg. 1985. Functional reconstitution of lens gap junction proteins into proteoliposomes. *Journal of Membrane Biology.* 85:87–92.

Noda, M., and S. F. Numa. 1987. Structure and function of sodium channel. *Journal of Receptor Research.* 7:467–497.

Okinami, S. 1978. Freeze-fracture replica of the primate lens fibers. *Albrecht Von Graefes Archiv für Klinische und Experimentelle Ophthalmologie.* 209:51–58.

Paul, D. L. 1986. Molecular cloning of cDNA for rat liver gap junction protein. *Journal of Cell Biology.* 103:123–134.

Paul, D. L., and D. A. Goodenough. 1983. Preparation, characterization, and localization of antisera against bovine MP26, an integral protein from lens fiber plasma membrane. *Journal of Cell Biology.* 96:625–632.

Peracchia, C. 1978. Calcium effects on gap junction structure and cell coupling. *Nature.* 271:669–671.

Peracchia, C., and S. J. Girsch. 1985. Is the C-terminal arm of lens gap junction channel protein the channel gate. *Biochemical and Biophysical Research Communications.* 133:688–695.

Peracchia, C., and L. L. Peracchia. 1980*a*. Gap junction dynamics: reversible effects of divalent cations. *Journal of Cell Biology.* 87:708–718.

Peracchia, C., and L. L. Peracchia. 1980*b*. Gap junction dynamics: reversible effects of hydrogen ions. *Journal of Cell Biology.* 87:719–727.

Philipson, B. T., L. Hanninen, and E. A. Balzas. 1975. Cell contacts in human and bovine lenses. *Experimental Eye Research.* 21:205–219.

Rae, J. L. 1979. The electrophysiology of the crystalline lens. *Current Topics in Eye Research.* 1:37–90.

Rae, J. L. 1985. The application of patch clamp methods to ocular epithelia. *Current Eye Research.* 4:409–420.

Rae, J. L., and J. R. Kuszak. 1983. The electrical coupling of epithelium and fibers in the frog lens. *Experimental Eye Research.* 36:317–326.

Rae, J. L., and R. A. Levis. 1984. Patch voltage clamp of lens epithelial cells: theory and practice. *Molecular Physiology.* 6:115–162.

Sas, D. F., M. J. Sas, K. R. Johnson, A. S. Menko, and R. G. Johnson. 1985. Junctions between lens fiber cells are labeled with a monoclonal antibody shown to be specific for MP26. *Journal of Cell Biology.* 100:216–225.

Scaglione, B. A., and D. A. Rintoul. 1989. A flourescence-quenching assay for measuring permeability of reconstituted lens MIP26. *Investigative Ophthalmology and Visual Science.* 30:961–966.

Scheutze, S. M., and D. A. Goodenough. 1982. Dye transfer between cells of the embryonic chick lens becomes less sensitive to CO_2 with development. *Journal of Cell Biology.* 92:694–705.

Simon, S. A., G. Zampighi, T. J. McIntosh, M. J. Costello, H. P. Ting beall, and J. D. Robertson. 1982. The structure of junctions between lens fiber cells. *Bioscience Reports.* 2:333–341.

Spray, D. C., A. L. Harris, and M. V. Bennett. 1981. Equilibrium properties of a voltage-dependent junctional conductance. *Journal of General Physiology.* 77:77–93.

Spray, D. C., J. C. Saez, D. Brosius, M. V. Bennett, and E. L. Hertzberg. 1986. Isolated liver gap junctions: gating of transjunctional currents is similar to that in intact pairs of rat hepatocytes. *Journal of Cell Biology.* 83:5494–5497.

Stroud, R. M. 1987. Topological mapping and the ionic channel in an acetylcholine receptor. *Society of General Physiologists Series.* 41:67–75.

Swenson, K. I., J. R. Jordan, E. C. Beyer, and D. L. Paul. 1989. Formation of gap junctions by expression of connexins in *Xenopus* oocyte pairs. *Cell.* 57:145–155.

Wong, M. M., N. P. Robertson, and J. Horwitz. 1978. Heat induced aggregation of the sodium dodecyl sulfate-solublizied main intrinsic polypeptide isolated from bovine lens plasma membrane. *Biochemical and Biophysical Research Communications.* 84:158–165.

Young, J. D., Z. A. Cohn, and N. B. Gilula. 1987. Functional assembly of gap junction conductance in lipid bilayers: demonstration that the 27 kd protein forms the junctional channel. *Cell.* 48:733–743.

Zampighi, G., J. M. Corless, and J. D. Robertson. 1980. On gap junction structure. *Journal of Cell Biology.* 86:190–198.

Zampighi, G., S. A. Simon, J. D. Robertson, T. J. McIntosh, and M. J. Costello. 1982. On the structural organization of isolated bovine lens fiber junctions. *Journal of Cell Biology.* 93:175–189.

Zampighi, G. A., J. E. Hall, G. R. Ehring, and S. A. Simon. 1989. The structural organization and protein composition of lens fiber junctions. *Journal of Cell Biology.* 108:2255–2276.

Zampighi, G. A., J. E. Hall, and M. Kreman. 1985. Purified lens junctional protein forms channels in planar lipid films. *Proceedings of the National Academy of Sciences of the United States of America.* 82:8468–8472.

Zimmer, D. B., C. R. Green, W. H. Evans, and N. B. Gilula. 1987. Topological analysis of the major protein in isolated intact rat liver gap junctions and gap junction-derived single membrane structures. *Journal of Biological Chemistry.* 262:7751–7763.